Spectral catalogue of bright gamma–ray bursts detected with the BeppoSAX/GRBM

C. Guidorzi[1], M. Lacapra[1], F. Frontera[1,2], E. Montanari[1,3], L. Amati[2], F. Calura[4], L. Nicastro[2], M. Orlandini[2]

[1] Dipartimento di Fisica, Università di Ferrara, via Saragat 1, I-44122 Ferrara, Italy
[2] INAF–IASF Bologna, via P. Gobetti 101, I-40129 Bologna, Italy
[3] Istituto IS Calvi, Finale Emilia (MO), Italy
[4] Jeremiah Horrocks Institute for Astrophysics and Supercomputing, University of Central Lancashire, Preston PR1 2HE, UK

ABSTRACT

Context. The emission process responsible for the so–called "prompt" emission of gamma–ray bursts is still unknown. A number of empirical models fitting the typical spectrum still lack a satisfactory interpretation. A few GRB spectral catalogues derived from past and present experiments are known in the literature and allow to tackle the issue of spectral properties of gamma–ray bursts on a statistical ground.
Aims. We extracted and studied the time–integrated photon spectra of the 200 brightest GRBs observed with the Gamma–Ray Burst Monitor which flew aboard the BeppoSAX mission (1996–2002) to provide an independent statistical characterisation of GRB spectra.
Methods. The spectra have a time-resolution of 128 s and consist of 240 energy channels covering the 40–700 keV energy band. The 200 brightest GRBs were selected from the complete catalogue of 1082 GRBs detected with the GRBM (Frontera et al. 2009), whose products are publicly available and can be browsed/retrieved using a dedicated web interface. The spectra were fit with three models: a simple power–law, a cut–off power law or a Band model. We derived the sample distributions of the best-fitting spectral parameters and investigated possible correlations between them. For a few, typically very long GRBs, we also provide a loose (128-s) time–resolved spectroscopic analysis.
Results. The typical photon spectrum of a bright GRB consists of a low–energy index around 1.0 and a peak energy of the νF_ν spectrum $E_p \simeq 240$ keV in agreement with previous results on a sample of bright CGRO/BATSE bursts. Spectra of $\sim 35\%$ of GRBs can be fit with a power–law with a photon index around 2, indicative of peak energies either close to or outside the GRBM energy boundaries. We confirm the correlation between E_p and fluence, in agreement with previous results, with a logarithmic dispersion of 0.13 around the power–law with index 0.21 ± 0.06. This is shallower than its analogous in the GRB rest–frame, the Amati relation, between the intrinsic peak energy and the isotropic–equivalent released energy (slope of ~ 0.5). The reason for this difference mainly lies in the instrumental selection effect connected with the finite energy range of the GRBM particularly at low energies.
Conclusions. We confirm the statistical properties of the low–energy and peak energy distributions found by other experiments. These properties are not yet systematically explained in the current literature with the proposed emission processes. The capability of measuring time–resolved spectra over a broadband energy range, ensuring precise measurements of parameters such as E_p, will be of key importance for future experiments.

Key words. gamma rays: bursts

1. Introduction

Giant leaps in the knowledge of the gamma-ray burst (GRB) explosions have been made in the last 15 years, mainly thanks to the discoveries obtained by former BeppoSAX (1996–2002), HETE–II (2000–2006) and current Swift (2004) and Fermi (2008) missions, as well as those made by ground facilities in response to the spacecraft triggers.

Time-integrated photon spectra of long GRBs can be adequately fit with a smoothly broken power–law (Band et al. 1993), whose low-energy and high-energy photon indices, α and β, have median values of -1 and -2.3, respectively (Preece et al. 2000; Kaneko et al. 2006; hereafter K06). Similar results were obtained by time-resolved spectral analysis (Frontera et al. 2000; Ghirlanda et al. 2002; K06). In spite of this, the nature and emission mechanisms responsible for the prompt emission of GRBs are still a matter of debate.

The corresponding νF_ν spectrum peaks at E_p, the so-called peak energy, whose rest-frame value is found to correlate with other relevant observed intrinsic properties, such as the isotropic-equivalent radiated γ-ray energy, E_{iso} (Amati et al. 2002), or its collimation-corrected value, E_γ (Ghirlanda et al. 2004). These correlations are observed to hold statistically on the sample of GRBs with known intrinsic quantities; however, they are affected by a significant dispersion, which could be due to some hidden variables. Specifically, while the scatter of the E_p–E_{iso} relation is well measured and known to differ from zero (e.g., Amati et al. 2009), the same issue for the corresponding collimation–corrected relation is debated (e.g., Campana et al. 2007; Ghirlanda et al. 2007; McBreen et al. 2010). In the BATSE catalogue (Paciesas et al. 1999), the E_p distribution clusters around 300 keV with a ~ 100 keV width (K06).

From the phenomenological perspective much effort has been made in order to characterise and identify typical spectral properties of bursts, by applying parametric spectral models that characterise, within the observational energy window, the

most relevant quantities. These quantities include the peak energy and the low and high energy components which are related, according to the most accredited emission theories, to the particle energy distribution and/or to the physical parameters of the emitting region.

One of the most promising mechanisms proposed for the gamma–ray emission is the synchrotron shock model (SSM). This model assumes that the electrons in an optically thin environment are accelerated by the first–order Fermi mechanism to a power–law distribution $dN(\gamma)/d\gamma \propto \gamma^{-p}$, where γ is the Lorentz factor. This distribution does not evolve in time, and the electron index p is related to the high–energy photon index either as $\beta = -(p + 2)/2$ in case of the fast–cooling synchrotron spectrum, or as $\beta = -(p + 1)/2$ in case of non-cooling synchrotron (Sari et al. 1998). The peak energy can be expressed as: $E_p \propto \gamma_e^2 B_{ps}$, where γ_e^2 is the pre–shock equilibrium electron energy and B_{ps} is the post–shock magnetic field (Tavani 1996).

The use of large catalogues represents a fruitful approach to the study of the spectral properties of GRBs on a statistical ground. In particular, the characterisation of the time–averaged photon spectra is important because it offers clues for understanding the radiation and particle acceleration mechanism at work during the prompt phase of GRBs, on which there is no consensus yet. In this paper, we extracted and studied the time–integrated photon spectra of the 200 brightest GRBs observed with the Gamma–Ray Burst Monitor (GRBM; Feroci et al. 1997; Frontera et al. 1997) aboard the BeppoSAX mission (Boella et al. 1997) and performed a novel statistical study of the main parameters characterising the GRB spectra.

The paper is organised as follows. Sections 2 and 3 report the observations, data reduction, and analysis. We report our results in Sect. 4, in the light of the models proposed in the literature, and Sect. 5 presents our discussion and conclusions.

All quoted errors are given at 90% confidence level for one interesting parameter ($\Delta\chi^2 = 2.706$), unless stated otherwise.

2. Observations

The GRB sample used for this analysis was extracted from the GRB catalogue of the BeppoSAX/GRBM (Frontera et al. 2009, hereafter, F09). The main constraints in the selection process were the following:

– sufficient number of total counts on the most illuminated detector unit;
– well defined response function, connected with the information on the GRB arrival direction;
– reliable background interpolation.

In order to be able to derive a reliable time-integrated spectrum, we noted that the average threshold on the number of total counts for a given detector unit ranges from 3000 to 4000, depending on the GRB local direction to BeppoSAX and on the GRBM unit considered in each case.

A number of GRBs (28) have also been detected in common with BATSE, whose data were published by K06 (see Sect. 4.8). For these bursts, in addition to exploiting the information on the GRB position derived by BATSE, useful to choose the appropriate response function, we compared the results we obtained with the GRBM data with what published by K06.

The background interpolation and subtraction required the availability of spectra acquired within contiguous time intervals around that/those including the burst. This requirement further limited the final number of selected events.

Finally we ended up with 185 bright GRBs out of the 1082 GRBs belonging to the GRBM catalogue (F09). Hereafter, fluence Φ is referred to the 40–700 keV energy band, unless otherwise specified. The values of the largest and lowest fluences included in the final sample are 1.7×10^{-4} and 4.4×10^{-6} erg cm^{-2}, respectively.

3. Data reduction and analysis

Firstly, among the 128-s time intervals continuously sampled with a time-integrated spectrum, we identified those including the GRBs and those adjacent, required for the background estimate. In some cases we took only the most illuminated unit for each GRB; in the remaining cases, we considered the two most illuminated units, apart from a few cases, for which it was possible to extract meaningful spectra from three different units. The two-unit case typically occurred when the burst direction with respect to the BeppoSAX local frame was such as to give comparable counts to both units. Data from the second most illuminated unit were ignored when the signal-to-noise (S/N) did not allow a statistically significant spectral reconstruction.

Table 1 reports the details of the data available for each analysed burst: for each spectrum the corresponding time interval is referred to the on-ground trigger time (F09), expressed as seconds of day (SOD). Each spectrum of a given burst is tagged with a letter and the corresponding packet number inherited from the GRBM archival data (and used in the GRB catalogue web interface[1]) is also reported.

The GRB spectra reduction and analysis is performed as follows:

– dead-time correction of both source and background 128-s long spectra (Sect. 3.1);
– background fitting by interpolation of adjacent 128-s dead-time corrected spectra (Sect. 3.2);
– identification of the appropriate GRBM response function (dependent on the GRB position; Sect. 3.3);
– spectral fitting of background-subtracted GRB spectra:
  – GRB total spectrum ("time-integrated" spectrum);
  – individual 128-s spectra of the GRBs that happened to be split into two or more intervals ("time-resolved" spectra).

3.1. Dead-time correction

We set up the following procedure to correct the 128-s integrated spectra for dead time. The 40–700 keV light curve of the corresponding unit is taken into account because a nearly constant rate gives rise to a dead time effect smaller than a rate with prominent peaks of small time duration. For a given average 128 s spectrum, let $\tilde{c}_i$ be the observed counts in the 40–700 keV band for the i-th 1-s bin ($i = 1, \ldots, 128$). The dead-time corrected counts, c_i are calculated as $c_i = \tilde{c}_i/(1 - \tau\,\tilde{c}_i)$, where $\tau = 4\,\mu s$ is the dead time. Let f_i be the rate fraction of the corresponding bin, defined as $f_i = c_i/c$, where c is the sum of all c_i's ($i = 1, \ldots, 128$). Let $\tilde{s}$ the total number of measured counts in the 128-s spectrum integrated over the 240 energy channels; this must also satisfy the following:

$$\tilde{s} = \sum_{i=1}^{128} \frac{f_i\,s}{1 + \tau f_i\,s} \qquad (1)$$

where s is the number of the total corrected counts we would have observed integrating the spectrum in the absence of dead

---

[1] Available at http://saxgrbm.iasfbo.inaf.it
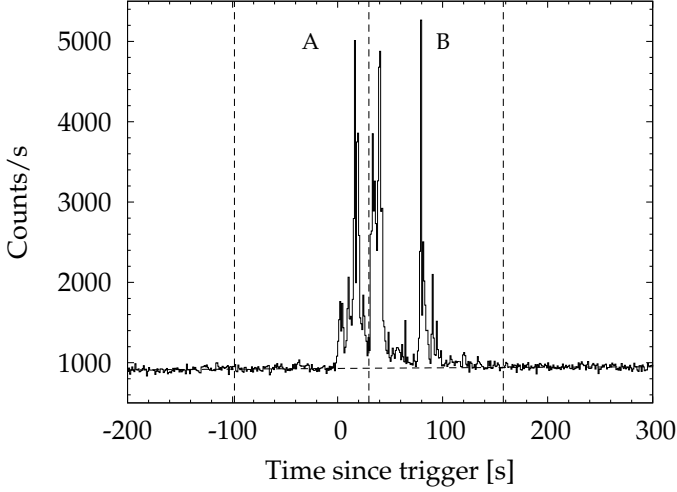
Fig. 1. 1-s light curve of GRB 000226 detected with GRBM unit 2 in the 40–700 keV band shown as an example. The dashed horizontal line shows the parabolic fit to the background. The vertical lines mark the time intervals corresponding to the 128-s spectra continuously acquired. Spectra "A" and "B" include the GRB, while the adjacent intervals are used to interpolate the background in each channel.

time. Therefore s can be estimated as the root of the following equation:

$$f(s) = \sum_{i=1}^{128} \frac{f_i s}{1 + \tau f_i s} - \tilde{s} = 0. \tag{2}$$

Assuming a negligible distortion of the original spectral shape due to dead time (which is the case when no strong spectral evolution occurs during the 128-s interval over which the spectrum is integrated), we renormalise the observed counts of each energy channel by the factor $s/\tilde{s}$.

3.2. Background subtraction

In order to reliably estimate the background counts in each energy channel of the time-integrated spectra, and to ensure a safe interpolation, we made sure that spectra accumulated over 128-s time intervals temporally contiguous to that including the burst were also available. In a few cases, either the time interval preceding or that following the GRB was not available; in these cases we checked that the background was so stable (typically within a few %) as to ensure linear (back)-extrapolation. For this reason we did not use the 128-s taken right before the ingress or right after the exit of a passage over the South Atlantic Anomaly.

Figure 1 shows the example of GRB 000226 (# 138 in Table 1). The independent spectral sampling happened to split this burst in two different 128-s spectra, called "A" and "B", respectively (marked by vertical lines). The light curve shown is the 40–700 keV profile of the most illuminated unit (GRBM 2): the background was interpolated with a parabolic fit (as in general), although a linear fit was already satisfactory. We identified the packet numbers corresponding to "A" and "B": 30 and 31, respectively. We also took two couples of adjacent spectra preceding (28, 29) and following (32, 33) the burst spectra, respectively. All these spectra were dead-time corrected as in Sect. 3.1.

At this point we performed two operations closely connected with one another: background fitting and energy channels' grouping. The latter operation is the result of ensuring
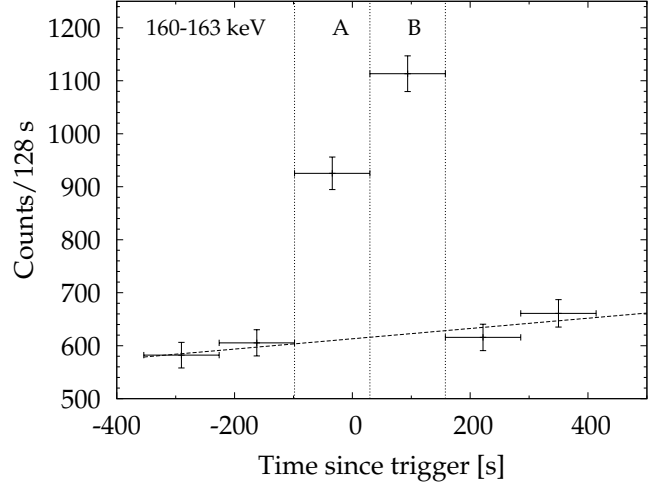
Fig. 2. 128-s light curve of energy channel 60 (160–163 keV) of GRB 000226 as seen with GRBM unit 2 (same example as in Fig. 1). The dashed line shows the linear fit of the background. Same vertical lines as in Fig. 1.

a minimum significance (3σ) on the net counts of the final background-subtracted grouped energy channel. More in detail, this is how the procedure works: it extracts the light curve of a given (original) energy channel out of the selected spectra. This light curve is then fit linearly (excluding the spectra including the GRB) so that the interpolated background counts expected during the GRB intervals are estimated. These steps are repeated for a sequence of adjacent energy channels: every time an original energy channel is summed up, the light curve extraction and fitting is reiterated for the grouped energy channel, until the total net counts exceed the significance threshold. When this is the case, the used energy channels are grouped into a final single channel. An example of this is displayed in Fig. 2 for the same burst shown in Fig. 1: the light curve of energy channel 60 (in this case corresponding to the energy range 160–163 keV) is built up from 6 contiguous 128-s time intervals. A satisfactory linear fit is performed on the background intervals (dashed line): the resulting net counts in the GRB intervals ("A" and "B") match the significance requirement so that this channel can stand alone.

The above steps are repeated until the full range of energy channels is covered. The last grouped channel, that in general does not fulfil the significance requirement, is merged into the previous one. The goodness of the fit of the background light curve for each grouped energy channel is expressed in terms of reduced χ^2. This is then checked by the human operator to make sure that all the fits are acceptable. The uncertainty on the net counts of each grouped channel is calculated by propagating the statistical uncertainties of counts and those affecting the interpolated background.

All this applies to the meaningful channels, i.e. from 18 to 240 out of the 256 nominal channels, while the remaining are ignored.

3.3. Response Matrices

The knowledge of the appropriate response matrices for a given burst requires the GRB position with respect to the BeppoSAX reference frame to be known, also called "local" position. The reason is the complex dependence of the response function on the local direction and photon energy, due to the BeppoSAX

payload itself surrounding the GRBM units. The GRBM response function for a generic direction was determined with Monte Carlo techniques (Calura et al. 2000) and in-flight calibrated with Crab observations and cross-calibrated with BATSE through commonly detected GRBs. See F09 for a detailed description.

The information on the directions of the GRBs considered in this work was taken from F09: column "CAT" in Table 1 reports the ID of the catalogue providing the most accurate position of each GRB using the same convention as in F09. For those GRBs for which no such information is available, typically the GRBs detected by the GRBM alone and for which the localisation procedure did not give a unique acceptable solution, we used as many response matrices as the possible directions and made sure that the spectral results were not significantly different from each other.

3.4. GRB spectra and models

In the case of GRBs whose profile was sampled by multiple 128-s intervals, we extracted and fit both the total (time-integrated) and the individual (time-resolved) spectra. Whenever the burst was contained within a single interval, no time-resolved spectrum was possible.

We adopted three possible fitting models: i) Band's model (BAND; Band et al. 1993) ii) the cut-off power–law (CPL), where the photon spectrum is $N(E) \propto E^{-\alpha} \exp\left[-E\,(2-\alpha)/E_p\right]$; iii) a simple power–law (POW), $N(E) \propto E^{-\alpha}$.

In addition to the normalisation, the free parameters of the fitting models were the power–law indices (the low- and high-energy α and β for BAND, only the low-energy index for the other models) and the peak energy, E_p, of the νF_ν spectrum. We note that the signs of the BAND photon indices follow a different convention from the other models. Spectral fitting was done using XSPEC v12.5 (Arnaud 1996).

Table 2 reports the spectral fitting results for the total spectra of all the bursts for various models. The POW model was adopted when the goodness of the fit, expressed through the reduced χ^2, was already acceptable and fitting with the other models did not provide any useful constraint on E_p. This was typically the case for bursts with the E_p either above or below the energy passband of the GRBM and/or for spectra with relatively poor S/N. Following Sakamoto et al. (2008a), for each of the 185 time-integrated spectra we first fit each spectrum with each of the three models. Whenever passing from a model to a more complex one the total χ^2 decreased by more than 6 for each additional degree of freedom, we considered it a significant improvement in modelling the spectrum (see Sakamoto et al. 2008a).

In most cases, the high-energy photon index β of the BAND function could not be constrained by the data, due to the narrower energy passband of the GRBM compared with that of BATSE as well as to the S/N ratio of the spectra. In such cases, we fixed its value to the average value of -2.3 found on the BATSE sample (K06). In a few cases the same problem occurred at low energies, for which we fixed the corresponding index α to the analogous value of -1.0.

We have not achieved in any case a statistical improvement with the BAND model, except for three cases of time-resolved spectra, characterised by a large S/N (spectra B of 980615B, 971208B and 970831). The best–fit model of each GRB is marked with an asterisk in Tables 2 and 3.

We excluded from statistical analysis the bursts whose spectra gave a poor fit, i.e. whose results in terms of χ^2/dof can be rejected at 99% confidence level. These cases represent less than
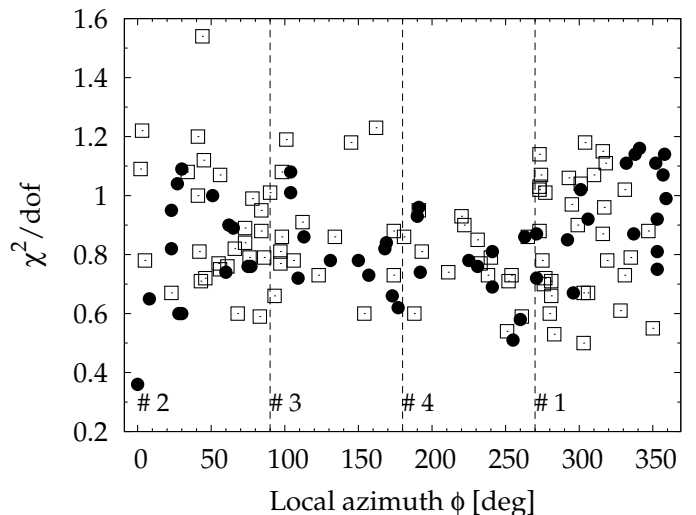
Fig. 3. Goodness of the fit for all the brightest GRBs with known arrival direction (143 out of 200) as a function of the BeppoSAX local azimuth angle ϕ. Vertical dashed lines at $\phi = 0°, 90°, 180°, 270°$ correspond to the axes of GRBM units 2, 3, 4, 1, respectively. Empty squares (filled circles) are the GRBs localised by other experiments (GRBM alone), as reported in F09.
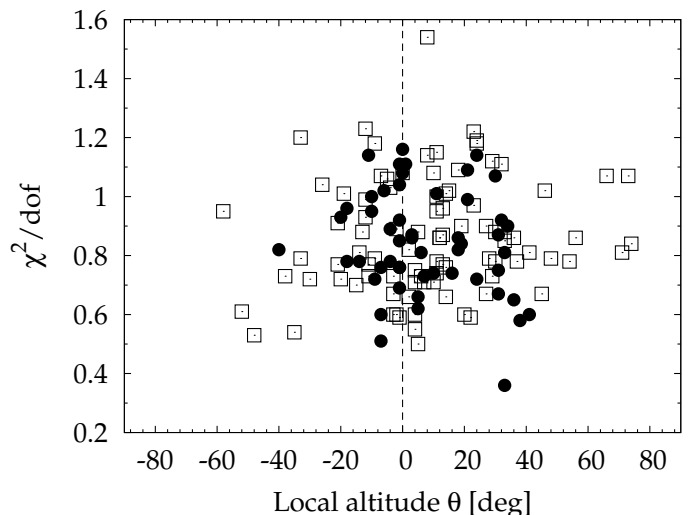
Fig. 4. Same as Fig. 3. Angle θ is the BeppoSAX local altitude above the equatorial plane, marked by the vertical dashed line.

3% of the total sample and are the following bursts: 980203B, 990118A, 000328, 001213 and 001228.

4. Results

4.1. Results in the BeppoSAX local frame

We studied the goodness of the spectral fit for each GRB as a function of the direction as referred to the BeppoSAX local frame of reference (F09). The aim is to check the goodness of the response matrix as a function of the GRB arrival direction. To this aim, we investigated how the total reduced χ^2 for each GRB best-fitting spectral model depends on both the local azimuth ϕ, measured counterclockwise from the axis of GRBM unit 2, and the local altitude θ above the BeppoSAX equatorial plane, respectively.

Figure 3 shows the reduced χ^2 of the best-fitting spectral model for each GRB as a function of the local azimuthal angle ϕ for 143 GRBs with known arrival direction out of our sample. The points are divided in two classes: those localised by other experiments (empty squares), whose information on the direction is independent from the GRBM, and the remaining ones localised with the GRBM (filled circles; see F09). Clearly both classes do not show any strong dependence of the goodness of the fit on the local azimuthal direction. We just note that GRBs close to GRBM unit 2 axis have slightly more scattered χ^2 values than other units.

Figure 4 shows the goodness of the fit as a function of the local elevation or altitude angle θ. As for the azimuthal angle, the goodness of the fit shows no dependence on the elevation angle either. Here noteworthy is the presence of more GRBs (60% of the total) in the BeppoSAX northern hemisphere ($\theta > 0°$): this is explained by the more effective absorption for southern directions due to the on-board electronics boxes in the lower part of the spacecraft (Guidorzi 2002), as evidenced by the number of bright GRBs, that drops significantly for elevation angles below $-20°/-30°$. The paucity of GRBM–localised GRBs compared with those localised by other instruments at directions close to the BeppoSAX local poles is due to the limitations of the GRBM localisation technique (F09).

4.2. Results of the pow model

The power–law model provides acceptable fits for $\sim 35\%$ of the sample. This model represents the best-fitting model for 10% of the 100 brightest GRBs; the same fraction rises to 53% when we consider the less bright half of the sample.

The power–law index α_{pow} distribution was derived by selecting only those GRBs whose spectral fitting gave an uncertainty smaller than 0.3. This choice was the result of a trade-off between the need of reasonably accurate values and the need of a good statistics. As a consequence the sample shrank to 87%.

The resulting distribution of α_{pow} can be fit with a Gaussian with $\overline{\alpha}_{\mathrm{pow}} = 1.86$ and $\sigma(\alpha_{\mathrm{pow}}) = 0.32$ (top panel of Fig. 5), in agreement within the analogous results obtained over a sample by Swift/BAT (1.6 ± 0.2; Sakamoto et al. 2008a) as well over a sample of INTEGRAL (1.6 in the energy band 18–300 keV; Vianello et al. 2009). The slightly softer average value we obtained with the GRBM bursts is explained by the harder energy range considered, thus more likely to be affected by the steepening of the spectrum due to the high-energy component; this conclusion is also supported by the corresponding value ($\overline{\alpha} \simeq 1.7$) obtained over the BATSE sample (K06).

The softness of most spectra fit with a pow model is explained with most GRBs having E_{p} below ~ 100 keV. About 30% of the pow indices lie in the range $1.7 < \alpha_{\mathrm{pow}} < 2.0$, so their peak energies are likely to lie close to the upper bound or above it, i.e. $E_{\mathrm{p}} \gtrsim 700$ keV. Another 37% of the same sample have $\alpha_{\mathrm{pow}} > 2$ and their peak energies lie at $E_{\mathrm{p}} < 40$ keV, as expected for the X–Ray Flashes (XRFs; Heise et al. 2001; Barraud et al. 2003; Sakamoto et al. 2005, 2008b; Pelangeon et al. 2008).

4.3. Results of the cpl model

Similarly to the pow model case, the distribution of the power–law index for the cpl model was derived selecting the GRBs with an uncertainty on α_{cpl} smaller than 0.5. 77% of the sample passed this criterion.
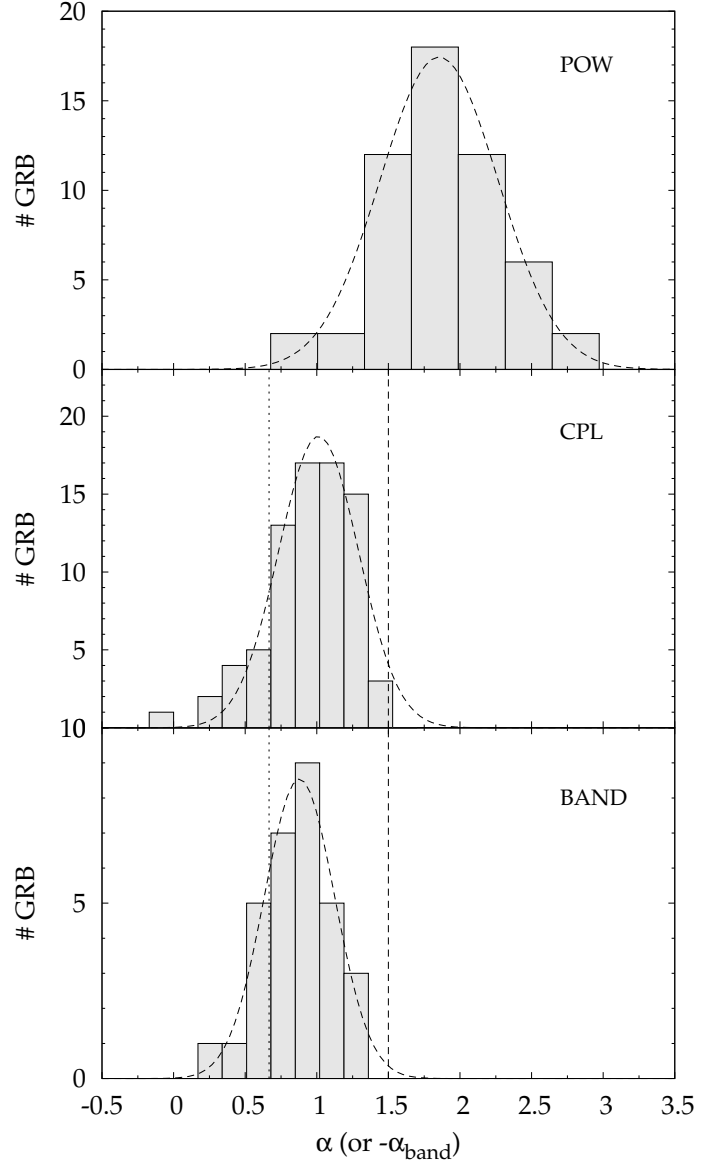
Fig. 5. *Top panel*: α_{pow} distribution for 55 GRBs with relative uncertainties smaller than 0.3. *Mid panel*: α_{cpl} distribution for 77 GRBs with relative uncertainties smaller than 0.5. *Bottom panel*: alternatively to the cpl model, we show the $-\alpha_{\mathrm{band}}$ distribution for 31 GRBs for which the band function provides an acceptable fit, although not significantly better than the cpl. The vertical dotted and dashed lines show the cases $\alpha = 2/3$ (synchrotron death line) and $\alpha = 3/2$ (cooling death line). In each panel dashed distributions show the corresponding best-fitting Gaussian functions.

The resulting distribution is fit with a Gaussian with mean and standard deviation values of $\overline{\alpha}_{\mathrm{cpl}} = 1.0$ and $\sigma(\alpha_{\mathrm{cpl}}) = 0.28$ (mid panel of Fig. 5).

Similar values were obtained from the observations of BAT aboard Swift: $\alpha_{\mathrm{cpl}} = 1.12 \pm 0.15$ (Cabrera et al. 2007), HETE-II: $\alpha_{\mathrm{cpl}} = 1.2 \pm 0.5$ (Barraud et al. 2003). There are no cases in which the low–energy index is very soft ($\alpha \geq 2$).

In the past, spectral fitting of time–resolved BATSE spectra of bright GRBs has yielded a significant number of cases with low–energy photon indices α below 2/3. This result is inconsistent with the SSM and $\alpha = 2/3$ has been referred to as its "death line" (Preece et al. 1998, Papathanassiou 1999 and refer-
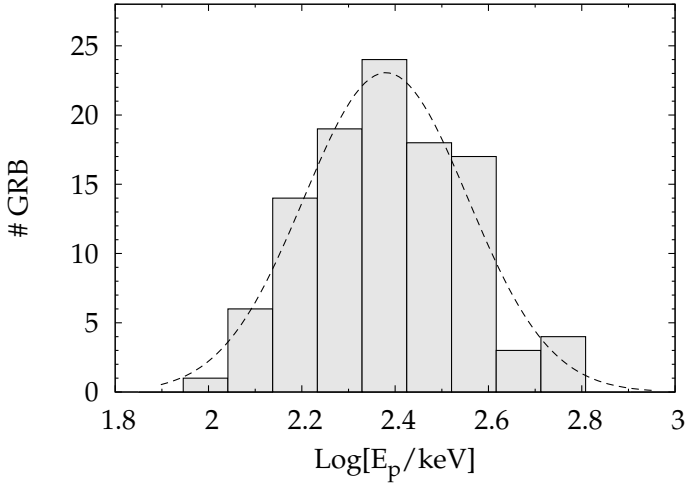
Fig. 6. Peak energy distribution derived with the CPL model for a sample of 106 GRBs with a relative uncertainty smaller than 40%. The dashed line shows the best-fitting normal distribution.

Fig. 7. Low–energy photon index vs. peak energy as determined with the CPL model on a sample of 70 GRBs with relatively accurate measurements.

ences therein). Our results indicate that about 30% of them lie below the synchrotron death line of $\alpha = 2/3$ (vertical dotted line in Fig. 5). On the other side of the distribution, no GRB lie beyond the fast-cooling death line (Ghisellini et al. 2000) represented by the limit $\alpha < 3/2$ (vertical dashed line).

Figure 6 shows the E_p distribution for the CPL model. Only values with uncertainties smaller than 40% are displayed; they represent 90% of the overall set of GRBs best fit with CPL. The distribution can be fit with a log–normal with mean and standard deviation of $\log E_p = 2.38 \pm 0.18$ (corresponding to a mode of $E_p = 240$ keV), fully consistent with the results obtained over a sample of bright BATSE bursts by K06: they found $E_p = 251^{+122}_{-68}$ keV using different fitting models.

Comparing the E_p distribution of our sample with the analogous of the BATSE GRBs fit only with the CPL model ($E_p = 321^{+202}_{-105}$ keV), although formally consistent with one another, suggests that the GRBM distribution is shifted towards lower values: this is primarily explained by the BATSE sensitivity at energies > 700 keV. The consequence of this selection effect is that a number of bright GRBs detected with the GRBM and with $E_p \gtrsim 700$ keV are clearly missing in the observed E_p distribution of Fig. 6, and belong to the GRBs that were fit with a power–law with $\alpha_{pow} < 2$.

We do not observe a sizable fraction of GRBs with $E_p < 100$ keV because our sample collects the brightest end of the GRBM fluence distribution: as a consequence, our sample is biased towards GRBs with high E_p values, because of its correlation with the fluence (Fig. 10).

We analysed the possible relation (if any) between α_{cpl} and E_p for a sample of 70 GRBs with both measurements sufficiently accurate by adopting the same thresholds mentioned above (0.5 on α_{cpl} and 40% on E_p). Figure 7 shows this sample in the α_{cpl}–E_p plane. A statistical study of our data shows no clear evidence for a correlation between these two quantities. In fact, the Spearman rank–order correlation coefficient over the whole sample turned out to be $r_s = -0.15$ with an associated probability of 21% of no correlation. However, for the low peak energy subsample ($\log E_p/\mathrm{keV} < 2.4$) the probability drops to 0.6% ($r_s = -0.49$), suggesting that the softer the peak energy, the softer the photon index. This type of correlation is expected because of the instrumental effect coming into play whenever E_p lies close to the edge of the energy passband. When this is the
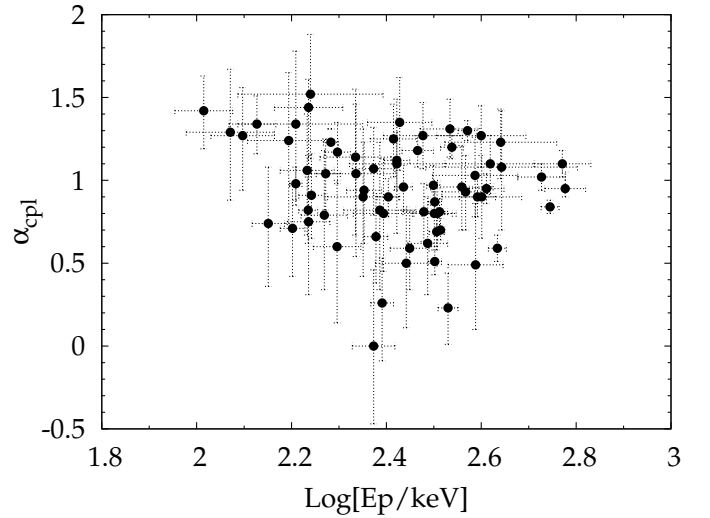
case, the low–energy photon index α as derived from the fitting procedure may have not reached the asymptotic value, thus resulting in a softer value (Preece et al. 1998; Lloyd & Petrosian 2000; Lloyd & Petrosian 2002; Amati et al. 2002). This is indeed what we observe in Fig. 7. That such a correlation seems to become significant when considering only the GRBs with low E_p values is a clear indication of its instrumental origin.

The number of GRBs whose α estimates are biased because of this effect depends on how smoothly the spectrum reaches its asymptotic value, in addition to the energy window of the detector. The same problem also affects samples of GRB spectra obtained with different detectors. To circumvent this issue, in the case of BATSE GRBs Preece et al. (1998) defined the "effective low–energy photon index" as the tangential slope at 25 keV (lower energy bound of BATSE detectors) of the spectrum in logarithmic scale. However, also with this definition the problem still remains whenever 25 keV is not low enough to reach the asymptote (Lloyd & Petrosian 2000). In our case, the impact on the α distribution shown in Fig. 5 is such that a few GRBs with $1.3 \lesssim \alpha_{cpl} \lesssim 1.5$ are likely to suffer from this effect. Different detectors with different energy windows should be also affected differently. However, as we noted above, the analogous distributions of other detectors, described by similar modes and dispersions, suggest that the impact of this instrumental effect on the observed α distribution is minimal.

4.4. Results of the BAND model

In none of the time–integrated spectra of our sample we found a significant improvement when changing the fitting model from CPL to BAND. Nevertheless, to explore how the choice of either model may affect the result, in the bottom panel of Fig. 5 we show the $-\alpha_{band}$ distribution for 31 GRBs for which the BAND function gave an acceptable result, although not significantly better than the CPL. Clearly, the two distributions are fully compatible with each other. In Section 4.7 we explore in more details the relation between the usage of the two models with our data.
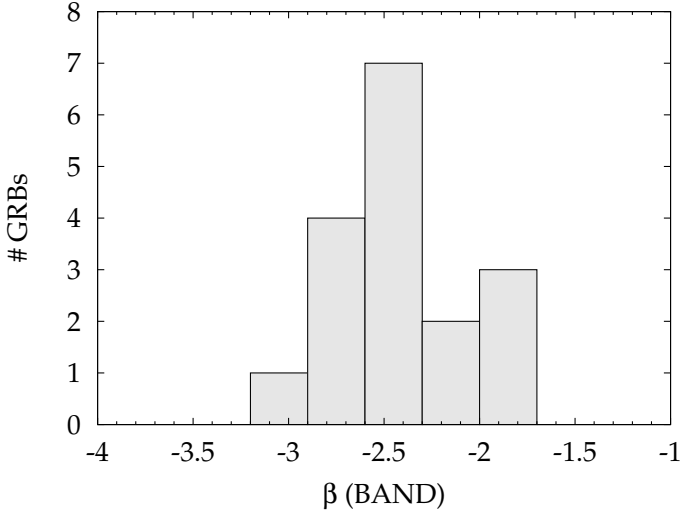
Fig. 8. High–energy photon index β distribution of the BAND function for a sample of 17 GRBs.

4.4.1. High–energy index

For a subsample of 17 GRBs out of the 31 mentioned above, it was also possible to constrain the high–energy photon index β with absolute uncertainties smaller than 1. The distribution is shown in Fig. 8. The small number of events for which this estimate was possible is explained by the relatively small upper bound of the GRBM passband compared with that of BATSE. However, we note that the resulting distribution is fully compatible with that derived on a more numerous BATSE sample (K06).

4.5. Fluence distribution

To account for the uncertainties in the response matrix calibration, we added in quadrature 10% systematic to the statistical fluence errors (F09). For each GRB we considered the fluence yielded by the corresponding best-fitting model. For the analysis we considered the mean value and symmetric error of the corresponding logarithms. The distributions of the best-fitting parameters and of the fluence were derived by excluding the GRBs affected by a relative uncertainty larger than 20% (after including the systematics); 12% of the sample were rejected as a consequence.

Figure 9 displays the cumulative fluence distribution (shaded histogram) compared with the corresponding distribution for 795 GRBs of the GRBM catalogue by F09, whose values were calculated through the 2-energy channel spectra (dashed histogram; see fig. 8 of F09). The solid line shows the power–law distribution with index $-3/2$, predicted in the case of no luminosity function evolution with redshift and where the observed GRBs are homogeneously distributed in the sampled volume of an Euclidean space. The difference between the observed and the predicted $-3/2$ power–law distributions had already been found in the BATSE catalogue (Meegan et al. 1992) and confirmed with the GRBM data (F09).

4.6. Peak energy–fluence correlation

Figure 10 displays the observed peak energy E_p vs. fluence Φ for a sample of 108 bright GRBs with well determined values. The correlation is significant: the Spearman rank coefficient is
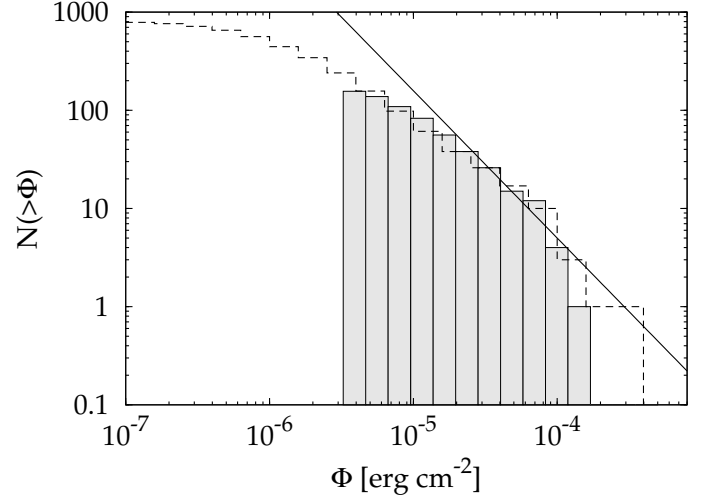
Fig. 9. Cumulative fluence distribution for the subset of GRBs with a relative error on fluence smaller than 20% (shaded histogram). The dashed histogram is the corresponding fluence distribution published by F09 for the entire GRBM catalogue of GRBs, as derived from 2–channel spectra. The solid line shows the power–law distribution with index $-3/2$ expected if GRBs were homogeneously distributed in an Euclidean space throughout the sampled volume.

$r_s = 0.48$ with an associated chance probability of 1.4×10^{-7}. Given the apparent scatter, we performed a power–law fit adopting the D'Agostini method (e.g., Guidorzi et al. 2006) and found the following best-fitting relation:

$$\log\left(\frac{E_p}{\text{keV}}\right) = (0.21 \pm 0.06) \log\left(\frac{\Phi}{\text{erg cm}^{-2}}\right) + (3.4 \pm 0.3) \quad (3)$$

The extrinsic scatter, which combines and must not be confused with the intrinsic scatter due to the uncertainties of the individual points, is $\sigma_{\log E_p} = 0.13 \pm 0.02$. The slope of the correlation agrees with previous values obtained on samples of BATSE GRBs (e.g. Lloyd, Petrosian & Mallozzi 2000; Nava et al. 2008). The scatter of each point in the E_p–Φ plane around the best-fit correlation is the result of the two sources of scatter: the intrinsic, different for each point and accounting for the uncertainties in the evaluation process of both observables, and the extrinsic scatter, reflecting a property of the correlation itself through some unknown variables. The combination of the two scatter sources finally give a normal distribution, as shown by the inset of Fig. 10: indeed the normalised scatter ζ_i, defined by eq. (4) with i running over the set of points, distributes according to a standardised Gaussian.

$$\zeta_i = \frac{y_i - (m\, x_i + q)}{\sqrt{\sigma_{y,i}^2 + m^2\, \sigma_{x,i}^2 + \sigma_y^2}} \quad (4)$$

where $y_i = \log E_{p,i}$, $x_i = \log \Phi_i$, the i-th σ's being the corresponding (intrinsic) uncertainties and σ_y being the extrinsic one. m and q are the best-fit slope and constant values reported in eq. (3), respectively.

It is known that truncation effects connected with the finiteness of the detector energy window may affect the distribution of the fitting parameters and the corresponding correlations. In particular, both E_p and fluence Φ suffer from them, as proven for BATSE GRBs by Lloyd, Petrosian & Mallozzi (2000), who investigated their impact in this respect. Our sample includes bright bursts, so truncation effects against low–fluence GRBs or near the detector threshold can be neglected.
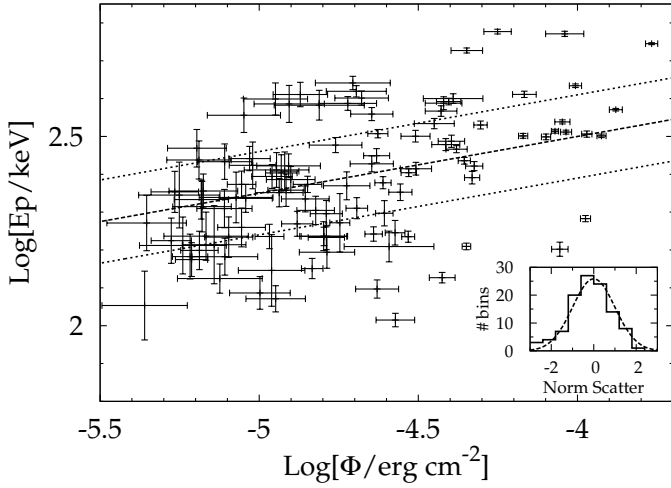
Fig. 10. Correlation between E_p and the 40–700 keV fluence for a sample of 108 bright GRBs with well determined values. The dashed line shows the best-fitting power–law, with index 0.21 ± 0.06, while the dotted lines include the 1-σ region, where $\sigma = 0.13$ is the extrinsic scatter. *Inset*: distribution of the normalised scatter. The dashed line shows the standardised normal distribution.

As discussed in Sect. 4.3, E_p is more likely to suffer from biases against low and high values (Lloyd & Petrosian 1999). Lloyd, Petrosian & Mallozzi (2000) tackled the issue of accounting for data truncation effects in the correlation studies by means of non–parametric techniques, which take into account the limits imposed by the detector in the determination of each parameter. Specifically for the E_p–Φ relation, they found similar results with these techniques and when considering the bright subsample of BATSE bursts, less affected than the GRBs close to the detector threshold. In both cases the value of the best-fitting slope (0.29 ± 0.03 and 0.28 ± 0.04, respectively) is similar to that found on our set. This suggests that the slope of the E_p–Φ correlation for the bright end of the GRBs detected with the GRBM is only marginally affected by this kind of truncation effects.

4.7. CPL vs. BAND

Although the BAND provided a significant improvement in the spectrum fitting only for a very few cases of time–resolved spectra (Sect. 3.4), we studied how the estimate of a given parameter compares with that obtained with the other model. In this respect, we considered both the low–energy photon index and the peak energy for a set of GRBs that could be fit with either model.

4.7.1. Peak Energy

Figure 11 shows the comparison of E_p as determined with the CPL and that derived with the BAND models for a sample of 63 GRBs for which both models provided an acceptable result. While for all GRBs they essentially provide consistent results within certainties, a linear regression accounting for the uncertainties of all the points along both axes shows that the CPL model tends to slightly overestimate E_p by $\sim 20\%$ on average with respect to the BAND function. This is proven by the best-fit (dotted line in Fig. 11) described by eq. (5).

$$\log E_{p,\mathrm{band}} = (1.012 \pm 0.042) \log E_{p,\mathrm{cpl}} - (0.077 \pm 0.102) \quad (5)$$
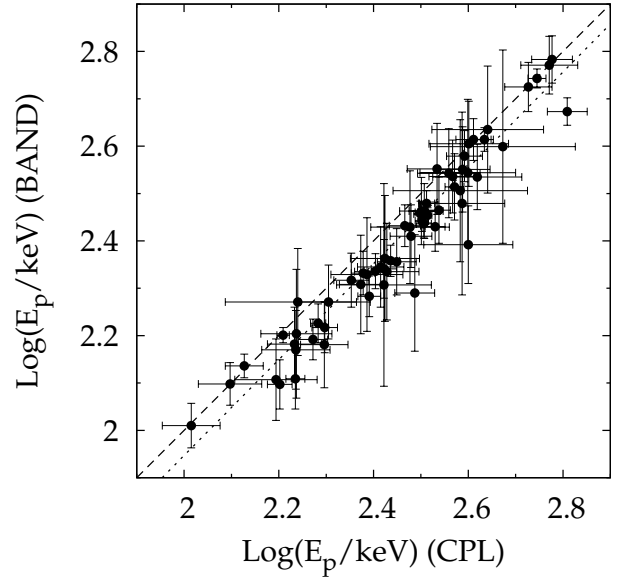
Fig. 11. Peak energy determined with the CPL vs. the same determined with the BAND function for a sample of 63 GRBs with both measurements. The dashed and dotted lines show the equality and the best-fitting power–law relations, respectively. In particular, according to the latter, the peak energy determined with the CPL tends to be $\sim 20\%$ larger than that of the BAND.

However, within the level of accuracy of our data, the two models provide equivalent estimates of E_p within uncertainties, as shown by the best-fitting parameters in eq. (5), fully consistent with equality.

4.7.2. Low–energy index

We selected a sample of GRBs with the low–energy photon index determined from the spectral fitting with both models and required both uncertainties to be smaller than 0.5. In this way 21 GRBs were selected, shown in Figure 12. For the sake of clarity, we consider $-\alpha_{\mathrm{band}}$ to be compared with α_{cpl}. The two models clearly provide consistent estimates for the low–energy photon index, as shown by the equality line (dashed). Performing a linear fit between the two sets taking into account the uncertainties along both axes, the result is described by eq. (6) and shown with dotted line in Fig. 12.

$$-\alpha_{\mathrm{band}} = (1.094 \pm 0.152)\, \alpha_{\mathrm{cpl}} - (0.145 \pm 0.146) \quad (6)$$

The slightly lower values of $|\alpha_{\mathrm{band}}|$ are not statistically significant, so in our sample we may consider the two models equivalent as for the low–energy photon index estimate.

4.8. GRBM vs. BATSE

In our sample there are 28 bursts observed also by BATSE whose spectral fitting results were published by K06; they are marked in Table 2.

For the sake of homogeneity, we considered the low–energy photon index values of BATSE obtained from fitting instead of the so–called effective values (Preece et al. 1998) estimated by K06. As shown in Fig. 13, the values of α of the GRBM sample look harder than BATSE, but this is not really significant and is merely due to the larger uncertainties of the former. There are a couple of cases with significantly different values for the two
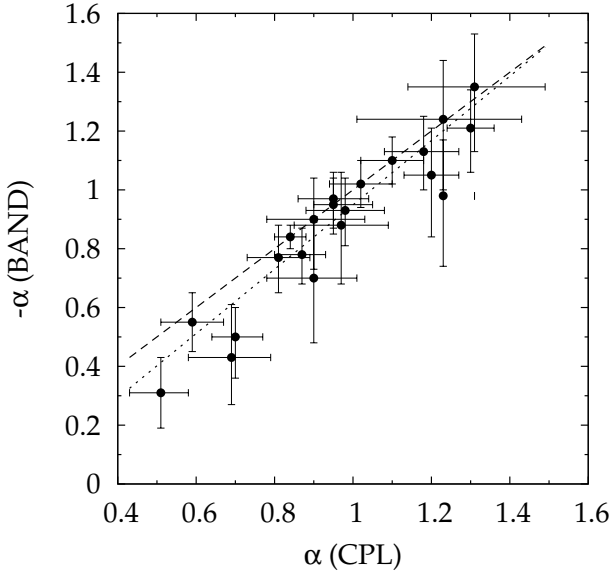
Fig. 12. Low–energy photon index determined with the CPL vs. the same determined with the BAND function for a sample of 21 GRBs with both measurements. The dashed and dotted lines show the equality and the best-fitting linear relations, respectively.
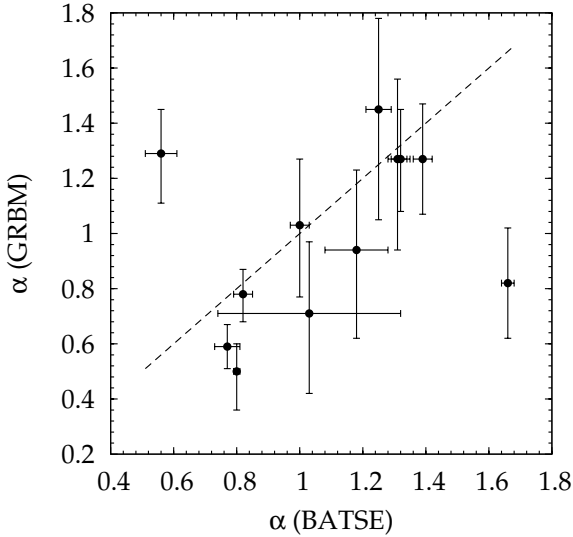
Fig. 13. BeppoSAX/GRBM versus BATSE: low-energy power–law spectra as measured with BAND and CPL models. The dashed line shows the equality line.

instruments: 970831 (4.2σ) and 971220 (4.4σ). We investigated the possible reasons for this discrepancy. In the case of 970831 K06's α is much softer than ours and this could be due to the different time intervals used: K06's spectrum missed the first $\sim$ 20 s of the $\simeq$ 150 s long burst. As for 971220, K06 integrated from BATSE trigger out to 9.5 s, whereas the burst lasted at least up to $\sim$ 15 s, missing the last part of the profile; the GRBM spectrum could be fit with a single power–law with $\alpha = 1.3 \pm 0.2$, consistent with the BATSE E_p of $\sim$ 2 MeV. However, their α estimate, taken from the CPL model, is reported to be $\alpha = 0.56 \pm 0.05$, i.e. much harder. Using the CPL by K06 might contribute to give a different value for α from that of the POW obtained by us; however this is due to the intrinsic curvature of the CPL.
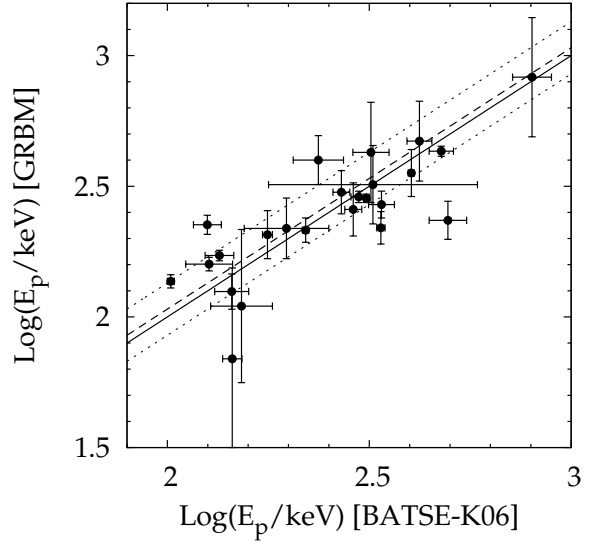
Fig. 14. BeppoSAX/GRBM versus BATSE: peak energy as measured with BAND and CPL models. The solid line shows the equality line. The dashed and dotted lines show the best-fitting relation and the $1-\sigma$ region.

Figure 14 displays the values of the peak energy for the sample of 28 common GRBs as determined from the two data sets. The points scatter around the equality line (solid): we quantified such scatter applying the D'Agostini method by fixing the slope of the relation to 1 and leaving the constant term as well as the extrinsic scatter free to vary. The best-fitting result is shown by the dashed line, whereas the dotted lines identify the $1-\sigma$ region around the best fit. Equation (7) describes the best-fitting function:

$$\log\left(\frac{E_{p,GRBM}}{keV}\right) = m \log\left(\frac{E_{p,BATSE}}{keV}\right) + q \tag{7}$$

The best-fitting values are $m = 1$ (fixed), $q = 0.03 \pm 0.05$, $\sigma(\log E_{p,GRBM}) = 0.10^{+0.07}_{-0.04}$. The origin of this scatter, corresponding to $\sim$ 26%, which adds in quadrature to the uncertainties of the individual points, must be searched in a combination of factors: i) the different integration time intervals, whose choice is forced by the different spectral sampling of the light curves of the two instruments; ii) the different energy passband; iii) different geometry GRB direction–Earth–instrument aboard the two spacecraft (with different albedo effects).

In practice, we note that an additional uncertainty of 26% in the time-average peak energy E_p estimate does not affect appreciably any correlation between E_p and other relevant observables, such as the $E_{p,i}$–E_{iso} relationship (Amati et al. 2002).

When we release the $m = 1$ constraint, we found a significant shallower dependence of $E_{p,GRBM}$ on $E_{p,BATSE}$, $m = 0.61 \pm 0.14$, not shown in Fig. 14. This is due to data truncation, as discussed in Sect. 4.6, and is explained by the narrower passband of the GRBM with respect to that of BATSE: the former tends to move inside the 40–700 keV range those values of E_p whose BATSE measurements, thanks to its broader energy range especially at high energies, are likely to be less biased by the finite energy range.

Even for E_p there are a few GRBs with significantly different values: 970616 (5.0σ), 971029 (4.8σ) and 990718 (3.8σ). The case of 970616 is peculiar, since it occurred when the BeppoSAX spacecraft was temporarily unstable due to the loss of gyroscopes in May–June 1997. As a consequence, the
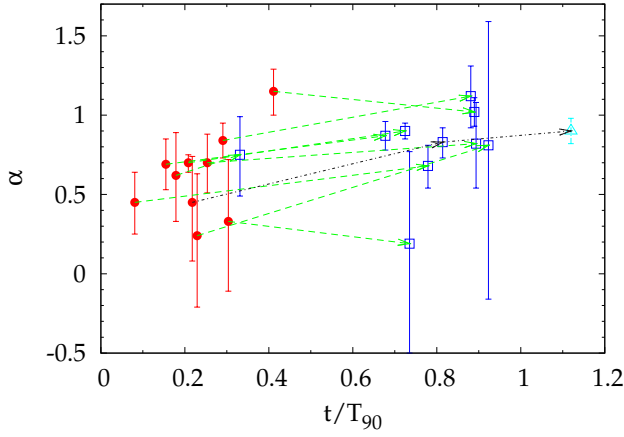
Fig. 15. Low–energy photon index as a function of time expressed in units of T_{90} for a subset of GRBs sampled by multiple spectral intervals. Filled circles, empty squares and triangles correspond to the spectra A, B and C, respectively. Each arrow tracks the evolution of a given GRB.

BeppoSAX local direction of this BATSE burst is not known and, even worse, throughout the duration of the burst (lasted about 80 s) the pointing was not constant. All this might have determined the discrepancy in the measurement of E_p, which is enhanced by the smallness of the uncertainties provided by K06: $E_{p,BATSE} = (102 \pm 2)$ keV to be compared with our $E_{p,GRBM} = (137 \pm 8)$ keV. The last case is that of 990718: clearly, the peak energy estimate by K06, $E_{p,BATSE} = (498 \pm 53)$ keV is much higher than ours, $E_{p,GRBM} = 232^{+45}_{-34}$ keV. We are confident that our results are more reliable. Indeed, while the GRBM spectrum covers the entire time profile, so does not that of K06: they missed the first and the last ~ 40 s of the overall profile. Missing the final soft tail of the light curve biased the E_p estimate towards harder values.

4.9. Time resolved spectra

We selected the GRBs whose time profiles have been sampled by multiple 128-s time intervals with spectral coverage. In particular we focused on the most common cases, i.e. when the total light curves split into two parts, called "A" and "B" (Fig. 1). We excluded those events whose total fluence has been split more inhomogeneously than 20%–80%. We ended up with a sample of 10 GRBs with reasonably well determined parameters with the CPL model. We added the case of 971110, which happened to be covered by three intervals that collected comparable fluences and with well determined parameters. Finally, we examined three very long GRBs that have been sampled by several (> 3) intervals and for which it was possible to extract at least three meaningful spectra each (Sect. 4.9.1).

Figures 15 and 16 show the temporal evolution of the low–energy photon index and of the peak energy, respectively, as a function of time. To account for the different durations of the GRBs in the subsample, time is conveniently expressed in units of T_{90} as measured by F09. The time assigned to each interval was calculated as the weighted-average over the 128 1–s bins, where the counts per bin in the light curve were used as the weights: for each interval this procedure identifies the time at which most of corresponding photons are observed. Filled circles and empty squares correspond to spectra "A" and "B", respectively. Dashed arrows connect points of the same GRB. The case of 971110 is highlighted with dark arrows. As can be
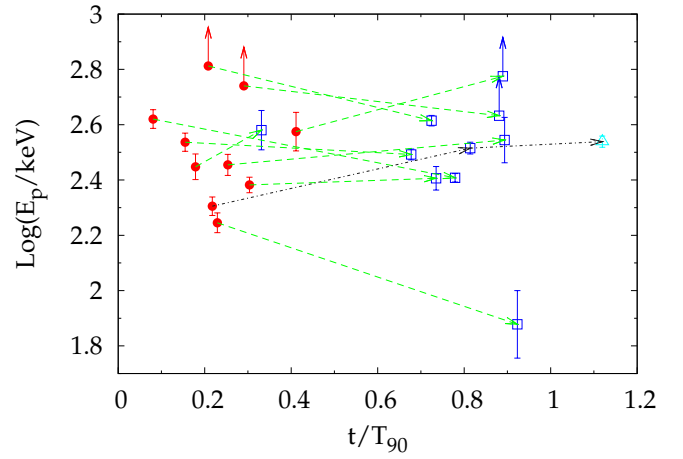
Fig. 16. Peak energy as a function of time expressed in units of T_{90}. Same as Fig. 15.
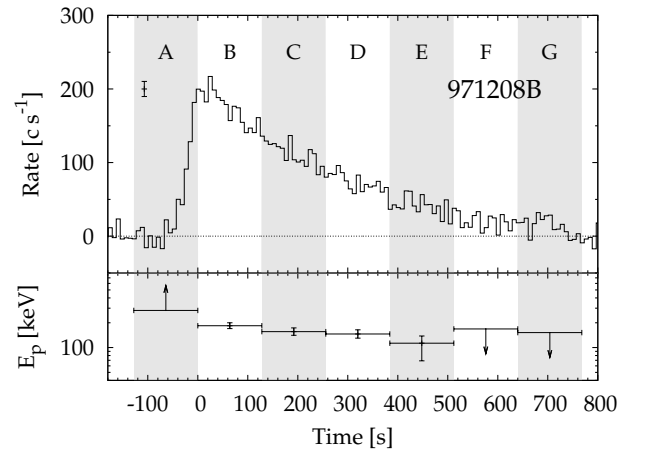
Fig. 17. *Top panel*: 40–700 keV time profile of 971208B. *Bottom panel*: peak energy evolution. Shaded area identify the different 128-s intervals over which an average spectrum was acquired.

seen, no global behaviour stands out. While Figure 15 suggests a marginal hard-to-soft evolution of the photon index, the peak energy (Fig. 16) shows all the possible cases compatibly with no standard evolution, in agreement with early observations of GRBs from past experiments (e.g., Kargatis et al. 1994; K06). The variety of the peak energy evolution throughout the time profile of a GRB is known to undergo a range of different behaviours: either tracking of the light curve or a steady hard–to–soft evolution are observed (e.g. see Peng et al. 2009a and references therein). It must be pointed out that these results are derived from a sample of bright GRBs and including fainter events could change the average evolution of the spectral parameters.

4.9.1. Very long GRBs

We examined three of the longest GRBs of our set, that happened to be sampled by several time intervals. For these GRBs we provide a more detailed analysis of how E_p evolves with time compared with the time profile. Figures 17, 18 and 19 show 971208B, 001213 and 010324, respectively: each top panel shows the 40–700 keV time profile with the typical error bar shown in the upper left corner, while the bottom panel shows the peak energy of the corresponding time intervals as a function of time. These GRBs confirm the variety of E_p evolution compared

Fig. 18. GRB 001213. Same plot as Fig. 17.

Fig. 19. GRB 010324. Same plot as Fig. 17.

Fig. 20. Peak energy vs. average flux for 971208B. The dashed line is the best-fitting power–law with a slope of 0.32 ± 0.15. Labelled spectra are the same as Fig. 17.

5. Discussion and Conclusions

We have analysed the spectral properties of the 185 brightest BeppoSAX/GRBM GRBs, using three different spectral models. The sample includes bright GRBs with a threshold on fluence of $\Phi > 4.4 \times 10^{-6}$ erg cm^{-2} in the 40–700 keV band; as a consequence, no short duration GRB was selected. The GRBM data used consist of 240–energy channel spectra in the 40–700 keV range continuously integrated over 128 s independently of the onboard trigger logic. For this reason, the analysis mainly concerned the time–integrated spectra of the GRBs; for a number of them, especially the very long ones, it was possible to carry out the spectral analysis for a few contiguous time intervals separately; these cases are referred to as time–resolved spectra.

About 35% of the sample are best fit with a power–law model (POW); the median value of the index is very close to 2. The analogous fraction for the Fermi/GBM, the brightest BATSE and the Swift known–z GRBs samples is 30%, 21% and 38%, respectively (Nava et al. 2010). The power–law index distribution is centred on $\alpha_{\rm pow} = 1.86 \pm 0.32$ and agrees with other experiments (Sakamoto et al. 2008a; Vianello et al. 2009). GRBs with $\alpha_{\rm pow} > 2$ ($\alpha_{\rm pow} < 2$) have a peak energy either close to or below (above) the GRBM lower (upper) bound, so $E_{\rm p} \lesssim 40$ keV ($E_{\rm p} \gtrsim 700$ keV).

The typical long and bright GRBs are well fit with either a cut–off power–law (CPL) or with a BAND function; with the GRBM data in none of the cases considered the latter model provided a significant improvement with respect to the former. We also proved that within the accuracy limits of these data, the two models provide consistent estimates for both the low–energy photon index α and the peak energy $E_{\rm p}$, although the CPL model tends to overestimate $E_{\rm p}$ with respect to the BAND function.

For a sample of 28 GRBs commonly detected by both GRBM and BATSE and for which K06 provided the results of the time-average spectral fitting, we carried out a comparative analysis to establish possible discrepancies and to evaluate the effects of measuring the same quantities with two different instruments. The two sets of α and $E_{\rm p}$ substantially agree with one another, except for a very few cases which we investigated and for which the main source of discrepancy must be searched in the different time coverage. A strong spectral evolution, observed for several GRBs, can explain why different time intervals may yield significantly different results in the spectral parameters. Specifically to $E_{\rm p}$, we modelled all these sources of

with the light curves: in the case of 971208B $E_{\rm p}$ steadily declined with time even during the rise of the single, long-lasting pulse. By contrast, in the other cases it remains roughly constant throughout different emitting episodes, followed by a final drop at the end of the prompt light curve.

Thanks to its very long duration, the case of 9701208B offers the opportunity to study the relation between the average flux and $E_{\rm p}$ in each interval. The result is shown in Fig. 20; the dashed line shows the best-fitting power–law relation, as parametrised by eq. (8):

$$\log\left(\frac{E_{\rm p}}{\rm keV}\right) = m \log\left(\frac{\rm Flux}{\rm erg\,cm^{-2}\,s^{-1}}\right) + q \qquad (8)$$

The best-fitting parameters computed over the four intervals with measured $E_{\rm p}$, from "B" to "E", are $m = 0.32 \pm 0.15$ and $q = 4.36 \pm 1.00$. Only spectrum "A" taken during the rise of the pulse is not compatible with the power–law model and this was already observed in other bursts with a broader energy coverage down to X–rays for a sample of bursts detected with both the Wield Field Cameras (WFC) and the GRBM aboard BeppoSAX (Frontera et al. 2010; Frontera et al. in prep.). This burst is also interesting because it belongs to the FRED (fast rise exponential decay) class, a family of bursts with a single pulse which are thought to be the building blocks of more complex time profiles (e.g. Norris et al. 1996). Similar results in the $E_{\rm p}$ evolution of FRED GRBs are discussed by Peng et al. (2009b).

discrepancy in terms of an additional scatter of about 26% between the GRBM and BATSE E_p estimates. In practice, this has little impact on the known correlations (Amati et al. 2002; Ghirlanda et al. 2004) in which E_p is a key observable.

The observed distribution of E_p peaks around 240 keV with a dispersion of 0.2 dex, very similar to that of bright BATSE bursts (K06; Nava et al. 2010). Its narrowness is explained by the finite passband of the GRBM as well as of the analogous experiments. That these selection effects connected with data truncation affect the distribution, as discussed in Sect. 4.3, is directly proven by analogous studies carried out over broader energy ranges. Indeed, in the X–ray domain (Frontera et al. 2000; Barraud et al. 2003; Amati 2006; Pelangeon et al. 2008; Sakamoto et al. 2008b) the number of X–ray rich GRBs and XRFs increases remarkably: as a result, the E_p distribution forms a continuum over a correspondingly broad energy band (Sakamoto et al. 2008b). Moreover, the selected sample is not representative of the entire population but only of the brightest end. A number of the GRBs included in our sample and best fit with a soft photon index are likely to have E_p between the XRFs and the hardest GRBs.

The α distribution has its mode around 1 with a dispersion of 0.32 (Fig. 5) very similar to the dispersion of 0.25 found for both low– and high–energy indices by K06 on a sample of bright BATSE GRBs. In this respect our results are in agreement with catalogues properties of other experiments (Preece et al. 2000; Ghirlanda et al. 2002; K06; Sakamoto et al. 2008a; Nava et al. 2010). For the GRBs with $E_p < 100 \div 150$ keV, α is poorly constrained and is slightly biased towards soft values (Fig. 7). As discussed in Sect. 4.3, this is due to an instrumental effect which limits the capability of correctly measuring the low–energy photon index when E_p lies close to the lower energy bound. For such GRBs, the spectrum cannot reach the asymptotic slope at the lower bound, so the value provided by the fitting procedure turns out to be softer than the asymptotic one (Lloyd & Petrosian 2000; Amati et al. 2002). How close the observed slope can be with respect to its asymptote depends on the spectrum itself and on its physical origin. For instance, assuming the validity of the synchrotron shock model, Lloyd & Petrosian (2000) studied how the smoothness of the cutoff in the electron energy distribution and the distribution of the pitch angle determine how quickly the asymptotic value of α is reached within a given energy passband.

As also noted by K06, the α distribution does not exhibit any clustering around characteristic values expected from various models: 2/3 for synchrotron with no cooling (Katz 1994; Cohen et al. 1997; Tavani 1996), 0 for jitter radiation expected in the case of synchrotron radiation in highly non–uniform short–scale magnetic fields (Medvedev 2000) and 3/2 for fast cooling synchrotron (Ghisellini et al. 2000).

About 30% of GRBs whose time–average spectrum is best fit with a cpl, lie below the synchrotron death line of $\alpha = 2/3$ (vertical dotted line in Fig. 5). This fraction is comparable to that found in BATSE GRB samples (Preece et al. 1998). On the other side of the distribution, the fast-cooling death line represented by the limit $\alpha < 3/2$ (vertical dashed line) is satisfied by all GRBs. However, the synchrotron process has several problems: the observed distribution around 1 is remarkably harder than 3/2 expected for a population of cooling electrons in the fast regime. Ghisellini et al. (2000) considered several options to overcome this discrepancy (particle re–acceleration, deviations from equipartition, quickly varying magnetic fields, adiabatic losses) concluding that the prompt spectrum could not be the result of ultrarelativistic electrons emitting synchrotron

and inverse Compton radiation. Alternatively, Lloyd & Petrosian (2000) found that spectra below the synchrotron death line are still possibly produced via synchrotron, provided that one assumes small pitch angles for the emitting electrons. Other possible explanations include synchrotron self–absorption in the X–ray (Granot et al. 2000), the presence of a photospheric component and pair formation (Meszaros & Rees 2000; Ioka et al. 2007), synchrotron self–Compton upscattered to X–rays from optical (Panaitescu & Meszaros 2000), time dependent acceleration and radiation (Lloyd & Petrosian 2002), the decay of magnetic fields (Pe'er & Zhang 2006), the Klein–Nishina effect on synchrotron self-Compton process (Derishev et al. 2001), or continuous electrons acceleration as a consequence of plasma turbulence in the post–shock region (Asano & Teresawa 2009).

We have confirmed the correlation between the observed peak energy E_p and the 40–700 keV fluence Φ with a null hypothesis probability of 1.4×10^{-7}. The slope of 0.21 ± 0.06 agrees with previous values obtained on samples of BATSE GRBs: 0.28 ± 0.04 (Lloyd, Petrosian & Mallozzi 2000), 0.16 ± 0.02 (Nava et al. 2008). The extrinsic scatter is $\sigma_{\log E_p} = 0.13 \pm 0.02$ (Fig. 10). The observed slope is likely to be only barely affected by data truncation and selection effects: in the literature, the same problem, affecting analogous samples from other experiments like BATSE, was circumvented by means of non–parametric techniques that had been set up to correct for data truncation. Furthermore, this was also done through the analysis of subsamples of brighter GRBs, less affected by selection effects due to the detector threshold, as is also the case of our sample. Results on the E_p–Φ correlation based on a proper treatment of these effects provided similar results on the correlation slope (see Lloyd, Petrosian & Mallozzi 2000 and references therein).

That the slope is shallower than ~ 0.5, slope of the intrinsic $E_{p,i}$–E_{iso} relation (Amati et al. 2002), is explained by a combination of different factors: i) in the observer frame, observables are not redshift–corrected. Due to the selection effects on E_{iso} with redshift (both observational and evolutionary), the farthest GRBs have the largest E_{iso}: this makes the E_p–Φ relation flatter than the intrinsic one. ii) The difficulty of detecting GRBs with E_p values either close to or below the lower bound of the GRBM passband of 40 keV, as suggested by Nava et al. (2008) in the case of BATSE, is an instrumental effect which limits the dynamical range, thus leading to a flatter slope. This seems to be confirmed by the results of Sakamoto et al. (2008b) who found a slope of 0.52 ± 0.11 for an extended sample of BATSE, HETE–II and Swift GRBs, much more sensitive to lower E_p than the GRBM alone. Although the extrinsic scatter found for the E_p–Φ relation is smaller than that of the intrinsic relation (~ 0.2), this must be compared with the dynamical range along E_p: moving from the observer to the intrinsic plane, the ratio between scatter and range along E_p significantly decreases, and the correlation becomes more significant (Amati et al. 2009).

In addition to the α distribution problem suffered by the synchrotron, the dependence of E_p on the prompt emission radius r is strong: assuming a fixed magnetic field fraction ϵ_B of the central luminosity L, it is $\epsilon_B L \simeq \Gamma^2 B^2 r^2 c$ (Γ is the bulk Lorentz factor of the baryonic outflow and B the magnetic field). If particles are accelerated at the shocks to random Lorentz factor γ, then E_p is expected to be:

$$E_p = \hbar \Gamma \gamma^2 \frac{e B}{m_e c} = \frac{e \hbar}{c^{3/2} m_e} \frac{\gamma^2}{r} \sqrt{\epsilon_B L} \simeq 100 \, r_{14}^{-1} \, L_{52}^{1/2} \text{ keV} \quad (9)$$

where we adopted the notation $Q = Q_n \times 10^n$ for a generic quantity Q and assumed $\gamma \sim m_p/m_e$. Equation (9) naturally

explains the $E_{p,i}$–L relation, i.e. the time-resolved version of the $E_{p,i}$–E_{iso} relation (Amati et al. 2002). However, relating r to the minimum observed variability timescale, $r \sim c\, t_v\, \Gamma^2$, implies the dependence of E_p on Γ, thus making the interpretation of the $E_{p,i}$–L_{iso} relation through eq. (9) troublesome. The resultant dependence of E_p on t_v is not observationally established (Lyutikov 2010). Recently, high-energy observations with Fermi of prompt-GeV correlated photons of GRB 080916C (Abdo et al. 2009a) would imply $r \sim 10^{16}$ cm (based on the constraints derived from the observations of GeV photons and minimum variability timescale in the light curve prompt), while the observed E_p of ~ 500 keV (Golenetskii et al. 2008) with time–resolved peaks up to a few MeV (Abdo et al. 2009a) is much larger than what expected from eq. (9). The same arguments hold for other high–energy GRBs detected with Fermi, such as GRB 090217A (Ackermann et al. 2010) and GRB 090902B (Abdo et al. 2009b).

Overall, the synchrotron shock model cannot account for the entire observed phenomenology of the GRB prompt emission (Kumar et al. 2007; Kumar & McMahon 2008; Kumar & Narayan 2009). Alternatively to the fireball model, in which most of the energy is initially bulk kinetic energy of a relativistic outflow turning into radiation through shocks, electromagnetic models have also been proposed in which the bulk energy is carried by magnetic fields and particle acceleration occurs through magnetic dissipation instead of shocks (Lyutikov 2006 and references therein).

More generally, the magnetic energy content of the ejecta can be explored effectively through early polarisation measurements, when most of the radiation comes from the ejecta themselves rather than the shocked interstellar medium as observed in the afterglow. At optical wavelengths this is thought to be the case whenever a reverse shock, which propagates through the ejecta, dominates the observed radiation during the γ–ray prompt emission or immediately afterwards (e.g., Zhang & Kobayashi 2005). This kind of measurements can discriminate between the possible different origins of the magnetic field: either a large–scale magnetic field originating at the central engine and carried forward by the ejecta, or a magnetic field generated in situ through the shocks. Although this kind of measurements is still in its infancy and more data are required to draw firm conclusions, early results on two recent bursts support the large–scale magnetic field scenario within ejecta with comparable magnetic and kinetic energy contents (Mundell et al. 2007; Steele et al. 2009).

Finally, for the longest GRBs it was possible to perform a time–resolved analysis with temporal resolution bound to 128 s. We confirmed the absence of a general evolution of the spectral parameters, especially E_p, throughout the GRB time profile: either a monotonic decline irrespective of the light curve or no remarkable evolution at all. In the case of 971208B, an almost 10^3–s long FRED, we tracked the spectral evolution in the E_p–flux observer plane, finding it consistent with the $E_{p,i}$–L relation (Yonetoku et al. 2004; Ghirlanda et al. 2005), except for the spectrum of the pulse rise, clearly incompatible with it (Fig. 20). This behaviour appears to be naturally explained in the context of synchrotron emission (eq. 9), although the issues mentioned above must be also considered. Tracking the peak energy evolution over a broader energy band down to X–rays will be crucial to better test the validity limits of this relation across individual GRBs as well as samples of GRBs and, consequently, to gain insight on the nature of the dominant emission process during the GRB itself. The importance of a broad band coverage is already shown by the time–resolved combined spectral study with WFC and GRBM aboard BeppoSAX on a sample of GRBs detected with both instruments (Frontera et al. 2010; Frontera et al. in prep.) as well as by the broadband spectral analysis of X–ray flares detected with Swift (Margutti et al. 2010). These capabilities will be of key importance with future missions like SVOM (Dong et al. 2010) and MIRAX (Braga & Mejía 2006; Braga et al. 2010).

References

Abdo, A.A., Ackermann, M., Arimoto, M. et al. 2009a, Science, 323, 1688
Abdo, A.A., Ackermann, M., Ajello, M. et al. 2009b, ApJ, 706, L138
Ackermann, M., Ajello, M., Baldini, M., et al. 2010, ApJ, 717, L127
Amati, L., Frontera, F., Tavani, M., et al. 2002, A&A, 390, 81
Amati, L. 2006, MNRAS, 372, 233
Amati, L., Frontera, F., Guidorzi, C. 2009, A&A, 508, 173
Arnaud, K., A., 1996, in Astronomical Society of the Pacific Conference Series, Vol. 101, Astronomical Data Analysis Software and Systems V, ed. G. H. Jacoby & J. Barnes, 17
Asano, K. & Teresawa, T. 2009, ApJ, 705, 1714
Band, D., Matteson, J., Ford, L., et al. 1993, ApJ, 413, 281
Barraud, C., Olive J.-F., Lestrade, J.P. et al. 2003, A&A, 400, 1021
Boella, G., Butler, R. C., Perola, G. C., et al. 1997, A&AS, 122, 299
Braga, J., Mejía, J. 2006, Proc. SPIE, 6266, 62660M
Braga, J., et al. 2010, IJMPD, Proc. of 2nd Galileo-Xu Guangqi Meeting, held in Villa Hanbury in July, 2010 , P. Chardonnet, L.-Z. Fang, R. Ruffini (Eds.), in press
Cabrera, J. I., Firmani, C., Avila-Reese, V., et al. 2007, MNRAS, 382, 342
Calura, F., Rapisarda, M., Frontera, F., et al., 2000, Proc. AIP, 526, 721
Campana, S., Guidorzi, C., Tagliaferri, et al., 2007, 472, 395
Cohen, E., Katz, J.I., Piran, T. et al. 1994, ApJ, 488, 330
Derishev, E.V., Kocharovsky, V.V., & Kocharovsky Vl.V. 2001, A&A, 372, 1071
Dong, Y.W., Wu, B.B., Li, Y.G., et al. 2010, Sc. Ch. G., 53, 40 (arXiv: 0907.2768)
Feroci, M., Frontera, F., Costa, E. et al. 1997, Proc. SPIE, 3114, 186
Frontera, F., Costa, E., Dal Fiume, D. et al. 1997, A&AS, 122, 357
Frontera, F., Amati, L., Costa, E. et al. 2000, ApJS, 127, 59
Frontera, F., Guidorzi, C., Montanari, E. et al. 2009, ApJS, 180, 192 (F09)
Frontera, F., Amati, L., Guidorzi, C., Landi, R., & La Parola, V. 2010, Mem. Soc. Astron. Italiana, 81, 426
Ghirlanda, G., Celotti, A., & Ghisellini, G. 2002, A&A, 393, 409
Ghirlanda, G., Ghisellini, G., & Lazzati, D. 2004, ApJ, 616, 331
Ghirlanda, G., Ghisellini, G., Firmani, C., Celotti, A. & Bosnjak, Z., 2005, MNRAS, 360, L45
Ghirlanda, G., Nava, L., Ghisellini, G., Firmani, A&A, 466, 127
Ghisellini, G., Celotti, A. & Lazzati, D. 2000, MNRAS, 313, L1
Golenetskii, H., Aptekar, R., Mazets, E., et al. 2008, GCN Circ., 8258
Granot, J., Piran, T. & Sari, R. 2000, ApJ, 534, L163
Guidorzi, C. 2002, PhD thesis, Univ. of Ferrara
Guidorzi, C., Frontera, F., Montanari, E. et al. 2006, MNRAS, 371, 843
Heise, J., in' t Zand, J., Kippen, R.M., & Woods, P.M. 2001, in Gamma-Ray Bursts in the Afterglow Era, ed. E. Costa, F. Frontera, & J. Hjorth (Berlin: Springer), 16
Ioka, K., Murase, K., Toma, K. et al. 2007, ApJ, 670, L77
Kargatis, V.E., Liang, E.P., Hurley, K.C., et al. 1994, ApJ, 422, 260
Kaneko, Y., Preece, R.D., Briggs, M.S., Paciesas, W.S., Meegan, C.A., Band, D.L. 2006, ApJS, 166, 298 (K06)
Katz, J.I. 1994, ApJ, 432, L107
Kumar, P., McMahon, E., Panaitescu, A., et al., 2007, MNRAS, 376, L57
Kumar, P. & McMahon, E., 2008, MNRAS384, 33
Kumar, P. & Narayan, R., 2009, MNRAS, 395, 472
Lloyd, N.M. & Petrosian, V. 1999, ApJ, 511, 550
Lloyd, N.M. & Petrosian, V. 2000, ApJ, 543, 722
Lloyd, N.M., Petrosian, V., Mallozzi, R.S. 2000, ApJ, 534, 227
Lloyd–Ronning, N.M. & Petrosian, V. 2002, ApJ, 565, 182
Lyutikov, M. 2006, New J. Phys., 8, 119
Lyutikov, M. 2010, Conf. Procs "The Shocking Universe meeting", Venice, G. Chincarini, P. D'Avanzo, R. Margutti and R. Salvaterra (Eds.), SIF, Bologna, Vol. 102, 3
Margutti, R., Guidorzi, C., Chincarini, G., M. G. Bernardini, F. Genet, J. Mao, F. Pasotti, 2010, MNRAS, 406, 2149

Mc Breen, S., Krühler, T., Rau, A., et al., 2010, A&A, 516, A71
Medvedev, M.V. 2000, ApJ, 540, 704
Meegan, C. A., Fishman, G. J., Wilson, R. B., et al., 1992, Nature, 355, 143
Meszaros, P. & Rees, M.J. 2000, ApJ, 530, 292
Mundell, C. G., Steele, I. A., Smith, R. J., et al. 2007, Science, 315, 1822
Nava, L., Ghirlanda, G., Ghisellini, G., and Firmani, C. 2008, MNRAS, 391, 629
Nava, L., Ghirlanda, G., Ghisellini, G., and Celotti, A. 2010, submitted
   (arXiv:1004.1410)
Norris, J.P., Nemiroff, R.J., Bonnell, J.T. 1996, ApJ, 459, 393
Paciesas, W.S., Meegan, C.A., Pendleton, G.N., et al., 1999, ApJS, 122, 465
Panaitescu, A. & Meszaros, P. 2000, ApJ, 544, L17
Papathanassiou H., 1999, A&AS, 138, 525
Pe'er, A. & Zhang, B. 2006, ApJ, 653, 454
Pelangeon, A., Atteia, J-L., Nakagawa, Y.E., et al. 2008, A&A, 491, 157
Peng, Z.Y., Ma, L., Lu, R.J., et al. 2009a, New A, 14, 311
Peng, Z.Y., Ma, L., Zhao, X.H. et al. 2009b, ApJ, 698, 417
Preece, R.D., Briggs, M.S., Mallozzi, R.S., Pendleton, G.N., Paciesas, W.S.,
   Band, D.L. 1998, ApJ, 506, L23
Preece, R.D., Briggs, M.S., Mallozzi, R.S., Pendleton, G.N., Paciesas, W.S.
   2000, ApJS, 126, 19
Sakamoto, T., Lamb, D. Q., Kawai, N., et al. 2005, ApJ, 629, 311
Sakamoto, T., Barthelmy, S.D., Barbier, L. et al. 2008a, ApJS, 175, 179
Sakamoto, T., Hullinger, D., Sato, G. et al. 2008b, ApJ, 679, 570
Sari, R., Piran, T., & Narayan, R. 1998, ApJ, 497, L17
Steele, I. A., Mundell, C. G., Smith R. J., Kobayashi, S., Guidorzi, C. 2009,
   Nature, 462, 767
Tavani, M., 1996, ApJ, 466, 768
Vianello, G., Götz, D., Mereghetti, S. 2009, A&A, 495, 1005
Yonetoku, D., Murakami, T., Nakamura, T., et al. 2004, ApJ, 609, 935
Zhang, B., Kobayashi, S. 2005, ApJ, 628, 315

Table 1. Log of the 128-s energy spectra of the brightest GRBM bursts. The SOD is measured in seconds of day of the on-ground trigger time (F09). The ID is a letter assigned to each spectrum of a given GRB.

#	GRB	SOD	ID	Packet	$t_{start}^{(a)}$	$t_{stop}^{(a)}$	T_{90}	units
-	-	(s)	-	#	(s)	(s)	(s)	-
1	960703	49374	A	29	-96.6	31.4	71	1 4 -
1	960703	49374	B	30	31.4	159.4	71	1 4 -
2	960707B	59186	A	2	-17.3	110.7	90	3 - -
3	960723A	17163	A	10	-55.2	72.7	54	2 - -
4	960805B	78957	A	14	-120.3	7.7	14	1 3 -
4	960805B	78957	B	15	7.7	135.7	14	1 3 -
5	960806	80916	A	8	-126.3	1.7	93	2 3 -
5	960806	80916	B	9	1.7	129.7	93	2 3 -
6	960825	01383	A	22	-62.1	65.9	114	2 1 -
6	960825	01383	B	23	65.9	193.9	114	2 1 -
7	960912	50248	A	6	-112.8	15.2	16	1 2 -
7	960912	50248	B	7	15.2	143.2	16	1 2 -
8	960917	80553	A	34	-118.4	9.5	18	1 4 -
8	960917	80553	B	35	9.5	137.5	18	1 4 -
9	960921	54229	A	10	-50.2	77.8	37	1 4 -
10	961022	68465	A	119	-87.1	40.9	27	1 - -
11	961208A	19457	A	18	-72.0	55.9	125	2 - -
11	961208A	19457	B	19	55.9	183.9	125	2 - -
12	961228	01798	A	12	-107.6	20.3	59	1 2 -
12	961228	01798	B	13	20.3	148.3	59	1 2 -
13	970111	35040	A	34	-67.2	60.8	31	3 - -
14	970116[b]	42081	-	-	-	-	-	- - -
15	970117B	53211	A	11	-108.3	19.7	13	1 2 -
15	970117B	53211	B	12	19.7	147.7	13	1 2 -
16	970122	42085	A	6	-16.7	111.2	49	2 - -
17	970203	05516	A	19	-6.0	122.0	72	1 - -
18	970228	10681	A	32	-38.8	89.2	56	1 - -
19	970307	70146	A	38	-61.1	67.0	21	2 4 -
20	970313	35158	A	36	-23.2	104.8	18	4 - -
21	970315A	56455	A	3	-48.3	79.7	15	2 3 -
22	970315B[b]	79759	-	-	-	-	-	- - -
23	970402	80316	A	35	-35.8	92.2	105	1 - -
23	970402	80316	B	36	92.2	220.2	105	1 - -
24	970420	72843	A	6	-114.3	13.7	9	1 4 -
25	970429	41784	A	37	-86.6	41.4	34	1 2 -
26	970509	48236	A	8	-37.8	90.1	55	3 4 -
27	970517B	32683	A	7	-43.1	84.9	5	2 3 -
28	970601[b]	69554	-	-	-	-	-	- - -
29	970603	35348	A	204	-110.6	17.4	45	2 3 -
29	970603	35348	B	205	17.4	145.4	45	2 3 -
30	970612B[b]	52106	-	-	-	-	-	- - -
31	970616	65439	A	21	-148.0	-20.0	64	1 - -
31	970616	65439	B	22	-20.0	108.0	64	1 - -
32	970624A	20705	A	208	-4.1	123.8	154	1 4 -
32	970624A	20705	B	209	123.8	251.8	154	1 4 -
33	970624B	23406	A	222	-121.1	6.8	12	1 - -
33	970624B	23406	B	223	6.8	134.8	12	1 - -
34	970625B	43986	A	296	-49.2	78.7	15	1 4 -
35	970627A[b]	25984	-	-	-	-	-	- - -
36	970627B[b]	79610	-	-	-	-	-	- - -
37	970704[b]	4097	-	-	-	-	-	- - -
38	970706	77997	A	162	-13.6	114.4	59	1 - -
39	970715	51671	A	12	-63.8	64.2	31	4 - -
40	970815[b]	43625	-	-	-	-	-	- - -
41	970816	08265	A	19	-20.7	107.3	6	1 2 -
42	970827B	35754	A	4	-93.1	34.9	78	2 3 -
42	970827B	35754	B	5	34.9	162.9	78	2 3 -
43	970831	63581	A	16	-132.1	-4.1	152	1 2 -
43	970831	63581	B	17	-4.1	123.9	152	1 2 -
44	970919B	65664	A	22	-30.8	97.3	33	2 3 -
45	970922A	02897	A	7	-50.8	77.2	32	2 3 -
46	971019	53753	A	32	-32.5	95.4	20	2 4 -
47	971022A	43038	A	36	-38.7	89.4	97	3 4 -
47	971022A	43038	B	37	89.4	217.4	97	3 4 -
48	971027A	09810	A	2	-117.8	10.2	11	1 2 -
48	971027A	09810	B	3	10.2	138.2	11	1 2 -
49	971029	05326	A	10	-15.9	112.1	92	3 4 -
50	971110	67990	A	27	-66.2	61.8	194	1 2 -
50	971110	67990	B	28	61.8	189.8	194	1 2 -
50	971110	67990	C	29	189.8	317.8	194	1 2 -
51	971114	44464	A	25	-31.4	96.6	98	3 4 -

Table 1. continued.

#	GRB	SOD	ID	Packet	$t_{start}^{(a)}$	$t_{stop}^{(a)}$	T_{90}	units
-	-	(s)	-	#	(s)	(s)	(s)	-
51	971114	44464	B	26	96.6	224.7	98	3 4 -
52	971122	77381	A	17	-63.5	64.5	63	1 - -
53	971127	00282	A	28	-96.7	31.3	23	1 2 -
54	971206B	69648	A	10	-119.0	9.0	42	1 - -
54	971206B	69648	B	11	9.0	137.0	42	1 - -
55	971208A	17232	A	31	-51.9	76.1	13	3 4 -
56	971208B	28116	A	19	-128.0	-0.0	456	3 - -
56	971208B	28116	B	20	-0.0	128.0	456	3 - -
56	971208B	28116	C	21	128.0	256.0	456	3 - -
56	971208B	28116	D	22	256.0	384.0	456	3 - -
56	971208B	28116	E	23	384.0	512.0	456	3 - -
56	971208B	28116	F	24	512.0	640.0	456	3 - -
56	971208B	28116	G	25	640.0	768.0	456	3 - -
57	971214B	84042	A	2	-90.5	37.5	30	1 - -
58	971220	14794	A	26	-19.2	108.9	12	1 3 4
59	971223C	38181	A	4	-118.9	9.1	47	2 3 -
59	971223C	38181	B	5	9.1	137.1	47	2 3 -
60	980105	02682	A	28	-37.1	90.9	37	1 - -
61	980124A	23676	A	39	-90.0	38.0	40	3 - -
62	980127	03532	A	8	-79.1	48.9	31	3 - -
63	980203B	82028	A	30	-47.2	80.7	23	2 3 -
64	980208B[(b)]	46260	-	-	-	-	-	- - -
65	980306B	34382	A	4	-36.1	91.9	-	2 3 -
65	980306B	34382	B	5	91.9	219.9	-	2 3 -
65	980306B	34382	C	6	219.9	347.9	-	2 3 -
66	980306C	63251	A	35	-10.1	117.9	21	2 3 -
67	980315B	26693	A	12	-70.5	57.6	105	1 - -
68	980321	21975	A	8	-40.1	88	166	1 2
68	980321	21975	B	9	88.0	216	166	1 2
69	980329A	13466	A	15	-91.6	36.4	19	3 - -
70	980403[(d)]	83752	-	-	-	-	-	- - -
71	980420	36412	A	24	-10.1	118.0	20	3 - -
72	980428	72608	A	5	-61.5	66.5	100	3 - -
72	980428	72608	B	6	66.5	194.5	100	3 - -
73	980516	41017	A	1	-45.2	82.8	16	1 2 -
74	980519A	13412	A	15	-15.7	112.3	33	1 2 -
75	980519B	44422	A	17	-110.7	17.3	28	3 - -
75	980519B	44422	B	18	17.3	145.3	28	3 - -
76	980615B	36736	A	28	-111.6	16.4	64	2 - -
76	980615B	36736	B	29	16.5	144.5	64	2 - -
77	980617	10312	A	10	-198.6	-70.6	186	2 4 -
77	980617	10312	B	11	-70.6	57.4	186	2 4 -
77	980617	10312	C	12	57.4	185.4	186	2 4 -
78	980624[(b)]	58073	-	-	-	-	-	- - -
79	980706B	57587	A	39	-32.3	95.7	71	2 3 -
80	980706D	78038	A	4	-2.3	125.7	146	1 4 -
80	980706D	78038	B	5	125.7	253.7	146	1 4 -
81	980709B	20407	A	27	-83.3	44.7	-	3 4 -
81	980709B	20407	B	27	44.7	172.6	-	3 4 -
82	980726[(b)]	60288	-	-	-	-	-	- - -
83	980728	31715	A	18	-127.9	0.1	52	2 3 -
83	980728	31715	B	19	0.1	128.1	52	2 3 -
84	980805[(e)]	49017	-	-	-	-	-	- - -
85	980808	28241	A	10	-114.3	13.7	140	2 - -
85	980808	28241	B	10	13.7	141.7	140	2 - -
86	980810B	66934	A	18	-63.4	64.6	-	3 - -
87	980827C	72625	A	17	-47.9	80.1	51	1 2 3
87	980827C	72625	B	18	80.1	208.1	51	1 2 3
88	981002	05466	A	30	-90.9	37.2	34	1 2 -
88	981002	05466	B	31	37.2	165.2	34	1 2 -
89	981018	01641	A	2	-69.3	58.7	115	3 - -
89	981018	01641	B	1	58.7	186.7	115	3 - -
90	981107[(b)]	779	-	-	-	-	-	- - -
91	981111	41371	A	22	-28.1	99.9	34	2 3 -
92	981125A	30383	A	2	-32.4	95.5	79	2 3 -
93	981125B	75981	A	18	-46.5	81.4	44	3 - -
94	981203A	03559	A	15	-124.7	3.3	142	3 4 -
94	981203A	03559	B	16	3.3	131.3	142	3 4 -
94	981203A	03559	C	17	131.3	259.3	142	3 4 -
95	981203B	26281	A	1	-107.8	20.2	65	1 2 -
95	981203B	26281	B	2	20.2	148.2	65	1 2 -
96	990117B	84976	A	24	-103.1	24.8	14	1 - -

Table 1. continued.

#	GRB	SOD	ID	Packet	$t_{start}^{(a)}$	$t_{stop}^{(a)}$	T_{90}	units
-	-	(s)	-	#	(s)	(s)	(s)	-
96	990117B	84976	B	25	24.8	152.8	14	1 - -
97	990118A	11562	A	30	-6.1	121.9	84	1 3 -
98	990123A	35230	A	9	-104.3	23.7	61	1 - -
98	990123A	35230	B	10	23.7	151.6	61	1 - -
99	990128	37252	A	15	-106.4	21.6	8	2 3 -
100	990131	70002	A	8	-128.5	-0.5	70	1 2 -
100	990131	70002	B	9	-0.5	127.5	70	1 2 -
101	990226	30888	A	7	-7.3	120.7	18	1 - -
102	990403A	08560	A	10	-34.5	93.6	83	1 2 -
103	990506A	41011	A	6	-70.5	57.6	129	3 4 -
103	990506A	41011	B	7	57.6	185.6	129	3 4 -
104	990510	31749	A	34	-67.6	60.4	57	3 - -
104	990510	31749	B	35	60.4	188.4	57	3 - -
105	990518B	62305	A	16	-25.8	102.1	32	1 - -
105	990518B	62305	B	17	102.1	230.1	32	1 - -
106	990521	83570	A	35	-24.0	104.0	33	3 4 -
107	990610	03784	A	10	-32.6	95.5	34	2 3 -
108	990620	81972	A	27	-45.6	82.4	16	2 3 -
109	990705	57685	A	8	-44.1	83.9	32	3 - -
110	990712A	27919	A	10	-98.3	29.7	38	2 - -
110	990712A	27919	B	11	29.7	157.7	38	2 - -
111	990712B	60182	A	17	-19.4	108.6	19	3 - -
112	990718	43613	A	28	-126.5	1.5	126	2 4 -
112	990718	43613	B	29	1.5	129.5	126	2 4 -
113	990720B	30591	A	21	-41.5	86.5	93	1 - -
114	990726	10773	A	3	-97.8	30.2	111	3 - -
114	990726	10773	B	4	30.2	158.3	111	3 - -
115	990907	63311	A	29	-74.0	54.0	145	3 - -
115	990907	63311	B	30	-54.0	182.0	145	3 - -
116	990913A	24716	A	11	-34.1	93.9	40	2 3 -
117	991104	61628	A	15	-71.8	56.2	32	1 4 -
118	991108	24365	A	10	-59.9	68.1	45	3 - -
119	991116	52265	A	32	-42.2	85.8	185	3 - -
119	991116	52265	B	33	85.8	213.9	185	3 - -
119	991116	52265	C	34	213.9	341.9	185	3 - -
120	991120	20810	A	26	-46.1	81.8	20	1 4 -
121	991122A	00386	A	11	-60.2	67.8	43	1 3 -
122	991124B	34270	A	33	-3.3	124.7	28	1 3 4
123	991205C	82661	A	22	-1.6	126.4	103	3 - -
124	991216B	58037	A	19	-97.0	31.0	15	4 - -
125	991221[c]	38196	-	-	-	-	23	1 2 -
126	991226A	54005	A	28	-114.3	13.7	18	3 - -
126	991226A	54005	B	29	13.7	141.7	18	3 - -
127	000104A	05324	A	40	-129.6	-1.5	55	1 - -
127	000104A	05324	B	41	-1.5	126.5	55	1 - -
128	000107C	78273	A	32	-35.6	92.4	38	2 - -
129	000109	37644	A	3	-16.7	111.3	142	2 4 -
129	000109	37644	B	4	111.3	239.3	142	2 4 -
130	000110	16725	A	32	-23.8	104.3	3	3 - -
131	000115	53372	A	30	-77.9	50.1	15	1 4 -
132	000119B	47373	A	32	-40.0	88.0	31	1 - -
133	000210	31445	A	5	-92.7	35.3	9	1 - -
134	000214A	03660	A	32	-27.8	100.2	8	1 - -
135	000218A	57670	A	20	-68.0	60.1	252	3 4 -
135	000218A	57670	B	21	60.1	188.1	252	3 4 -
135	000218A	57670	C	22	188.1	316.0	252	3 4 -
136	000218B	58745	A	28	-118.9	9.1	20	2 3 -
136	000218B	58745	B	29	9.1	137.1	20	2 3 -
137	000226	46268	A	30	-98.2	29.8	84	2 3 -
137	000226	46268	B	31	29.8	157.8	84	2 3 -
138	000227	77762	A	35	-109.3	18.7	102	2 4 -
138	000227	77762	B	36	18.7	146.7	102	2 4 -
139	000301C	45665	A	27	-141.3	-13.3	87	1 4 -
139	000301C	45665	B	28	-13.3	114.6	87	1 4 -
140	000312	19435	A	20	-124.5	3.5	24	1 2 -
140	000312	19435	B	21	3.5	131.5	24	1 2 -
141	000323	32526	A	33	-54.8	73.2	46	3 4 -
142	000327	81477	A	34	-110.1	18.0	87	2 3 -
142	000327	81477	B	35	18.0	146.0	87	2 3 -
143	000328	05709	A	20	-193.0	-65.0	116	1 2 -
143	000328	05709	B	21	-65.0	63.0	116	1 2 -
143	000328	05709	C	22	63.0	191.0	116	1 2 -
144	000419	07969	A	12	-90.7	37.3	20	2 3 -

Table 1. continued.

#	GRB	SOD	ID	Packet	$t_{start}^{(a)}$	$t_{stop}^{(a)}$	T_{90}	units
-	-	(s)	-	#	(s)	(s)	(s)	-
145	000420B	51731	A	2	-8.7	119.3	31	1 3 -
146	000421	44614	A	13	-100.7	27.3	44	3 4 -
146	000421	44614	B	14	27.3	155.2	44	3 4 -
147	000429	36442	A	8	-13.0	115.0	163	2 3 -
147	000429	36442	B	9	115.0	243.0	163	2 3 -
148	000523	68495	A	4	-38.8	89.2	-	2 3 -
148	000523	68495	B	5	89.2	217.2	-	2 3 -
149	000528	31584	A	12	-99.0	29.0	65	3 - -
149	000528	31584	B	13	29.0	157.0	65	3 - -
150	000615B	59555	A	5	-130.5	-2.5	18	2 - -
150	000615B	59555	B	6	-2.5	125.5	18	2 - -
151	000621	07251	A	9	-114.8	13.2	119	1 4 -
151	000621	07251	B	10	13.2	141.3	119	1 4 -
152	000630	01859	A	32	-95.0	33.0	26	1 2 -
153	000718B	74829	A	14	-84.0	44.0	34	2 - -
154	000727	70961	A	4	-101.3	26.7	-	2 - -
155	000811	55801	A	15	-125.8	2.2	51	4 - -
155	000811	55801	A	17	-125.8	2.2	51	1 - -
155	000811	55801	B	16	2.2	130.2	51	4 - -
155	000811	55801	B	18	2.2	130.2	51	1 - -
156	000904	47922	A	17	-67.5	60.5	10	1 4 -
157	000906	75649	A	1	-81.6	46.4	20	1 - -
158	001004	53486	A	2	-54.5	73.5	9	1 2 3
159	001011C	57288	A	5	-47.6	80.4	24	3 - -
160	001013	65618	A	28	-92.7	35.3	37	2 4 -
160	001013	65618	B	29	35.3	163.3	37	2 4 -
161	001019	86357	A	18	-93.9	34.1	28	1 2 -
162	001110	44249	A	5	-85.6	42.4	35	1 2 -
162	001110	44249	B	6	42.4	170.3	35	1 2 -
163	001115	50801	A	27	-49.9	78.1	134	4 - -
163	001115	50801	B	28	78.1	206.2	134	4 - -
164	001206A	34621	A	29	-122.5	5.5	41	1 - -
164	001206A	34621	B	30	5.5	133.5	41	1 - -
165	001206C	77380	A	28	-121.5	6.5	27	2 - -
165	001206C	77380	B	29	6.5	134.5	27	2 - -
166	001212A	34422	A	5	-2.7	125.3	116	1 2 -
167	001212B	53843	A	13	-34.7	93.3	67	2 4 -
168	001213	83225	A	7	-54.8	73.2	454	1 2 -
168	001213	83225	B	8	73.2	201.2	454	1 2 -
168	001213	83225	C	9	201.2	329.2	454	1 2 -
168	001213	83225	D	10	329.2	457.3	454	1 2 -
168	001213	83225	E	11	457.3	585.3	454	1 2 -
169	001217	58829	A	23	-66.8	61.2	69	3 - -
169	001217	58829	B	24	61.2	189.1	69	3 - -
170	001219A	27329	A	26	-60.9	67.1	234	4 - -
170	001219A	27329	B	27	67.1	195.1	234	4 - -
170	001219A	27329	C	28	195.1	323.1	234	4 - -
171	001228	43394	A	1	-71.2	56.8	13	1 2 -
172	010109	09486	A	26	-92.6	35.4	7	1 2 -
173	010119A	01195	A	7	-53.0	75.0	-	4 - -
174	010127	30558	A	33	-32.2	95.8	147	1 4 -
174	010127	30558	B	34	95.8	223.8	147	1 4 -
175	010213	10643	A	6	-60.7	67.2	10	3 - -
176	010222A	26583	A	31	-129.0	-1.0	74	1 - -
176	010222A	26583	B	32	-1.0	126.9	74	1 - -
177	010226A	69313	A	2	-85.2	42.7	20	1 - -
178	010317	23287	A	27	-5.8	122.2	30	2 3 -
179	010324	41548	A	15	-139.1	-11.1	292	1 2 -
179	010324	41548	B	16	-11.1	116.9	292	1 2 -
179	010324	41548	C	17	116.9	244.9	292	1 2 -
179	010324	41548	D	18	244.9	372.9	292	1 2 -
180	010326	11696	A	31	-120.1	7.9	19	1 2 4
180	010326	11696	B	32	7.9	135.9	19	1 2 4
181	010408B	24322	A	11	-88.6	39.4	4	1 2 -
182	010412	78389	A	27	-44.7	83.3	60	1 - -
183	010418	29523	A	14	-82.9	45.1	70	1 2 -
184	010427B	33604	A	4	-109.9	18.1	42	1 2 -
184	010427B	33604	B	5	18.1	146.1	42	1 2 -
185	010504	09826	A	5	-3.2	124.8	15	2 4 -
186	010517	85893	A	12	-11.6	116.3	37	1 - -
187	010521	24050	A	29	-118.8	9.2	34	2 3 -
187	010521	24050	A	30	9.2	137.2	34	2 3 -
188	010619	97106	A	19	-54.8	73.2	449	2 3 -

Table 1. continued.

#	GRB	SOD	ID	Packet	$t_{start}^{(a)}$	$t_{stop}^{(a)}$	T_{90}	units
-	-	(s)	-	#	(s)	(s)	(s)	-
188	010619	97106	B	20	73.2	201.2	449	2 3 -
188	010619	97106	C	21	201.2	329.2	449	2 3 -
188	010619	97106	D	22	329.2	457.2	449	2 3 -
189	010710B	84853	A	15	-79.4	48.6	20	2 4 -
190	010711	09830	A	14	-49.4	78.5	68	1 2 -
190	010711	09830	B	15	78.5	206.5	68	1 2 -
191	010715	73421	A	17	-126.6	1.4	45	2 3 -
191	010715	73421	B	18	1.4	129.4	45	2 3 -
192	010721	14211	A	21	-68.7	59.3	5	2 3 -
193	010801	66633	A	34	-77.2	50.8	42	1 2 -
194	010804	72798	A	8	-40.3	87.8	14	2 3 -
195	010813	35036	A	15	-31.6	96.4	-	2 4 -
196	010818A	49990	A	8	-58.7	69.3	41	1 4 -
197	010826	65161	A	10	-50.0	78.0	288	1 4 -
197	010826	65161	B	11	78.0	206.0	288	1 4 -
197	010826	65161	C	12	206.0	334.0	288	1 4 -
198	010921	18950	A	32	-56.7	71.4	22	2 4 -
199	010922	63412	A	5	-56.8	71.2	40	2 3 -
200	011003	12848	A	30	-11.0	117.0	34	1 2 -

[a] Time is referred to the on-ground trigger time SOD (third column).
[b] Unavailable data packets.
[c] Unknown start and end times.
[d] Low signal.
[e] Bad spectra.

Table 2. Spectral fitting results of the time-integrated spectra for each bright GRB. Spectral models used are: Band's model (BAND), the cut-off power–law (CPL) and the simple power–law (POW). α and β are the low- and high-energy photon indices (β is not defined for the CPL and POW models). E_p is the peak energy of the $\nu F \nu$ spectrum. CAT is the catalogue ID which provided the most accurate position for the GRB and is taken from Frontera et al. (2009). Frozen values are reported among square brackets. For each GRB the best–fit model is marked with an asterisk.

# GRB	GRB	model	α	β	E_p (keV)	$\Phi(40-700)$ (10^{-5} erg cm^{-2})	χ^2/dof	CAT	comment
-	-	-	-	-	(keV)	(10^{-5} erg cm^{-2})	-	-	-
1	960703	CPL	$1.45^{+0.33}_{-0.40}$	-	> 264	1.23 ± 0.10	0.77	4B 5526	K06; only unit 1 used
1	960703	POW (*)	$1.71^{+0.11}_{-0.11}$	-	-	1.26 ± 0.08	0.78	4B 5526	K06; only unit 1 used
2	960707B	CPL	$0.67^{+1.06}_{-1.68}$	-	> 180	0.40 ± 0.10	0.81	4B 5532	
2	960707B	POW (*)	$1.67^{+0.27}_{-0.27}$	-	-	0.46 ± 0.07	0.88	4B 5532	
3	960723A	CPL (*)	$0.25^{+1.31}_{-1.93}$	-	120^{+34}_{-37}	0.45 ± 0.09	0.55	4B 5551 -	
3	960723A	POW	$2.17^{+0.26}_{-0.25}$	-	-	0.55 ± 0.09	0.90	4B 5551	
4	960805B	CPL (*)	$0.12^{+0.56}_{-0.69}$	-	176^{+13}_{-12}	2.68 ± 0.20	1.06	-	
5	960806	POW (*)	$1.80^{+0.18}_{-0.18}$	-	-	1.44 ± 0.14	1.20	4B 5566	
6	960825	BAND	$1.60^{+1.30}_{-0.93}$	$-2.60^{+0.20}_{-0.20}$	191^{+21}_{-17}	4.41 ± 0.21	0.62	G	
6	960825	CPL (*)	$0.26^{+0.27}_{-0.35}$	-	246^{+14}_{-13}	4.67 ± 0.18	0.66	G	
7	960912	CPL	$1.15^{+0.56}_{-0.73}$	-	201^{+122}_{-46}	0.78 ± 0.10	0.89	4B 5601	
7	960912	POW (*)	$1.88^{+0.15}_{-0.14}$	-	-	0.86 ± 0.08	0.97	4B 5601	
8	960917	CPL (*)	$0.68^{+0.78}_{-1.01}$	-	214^{+71}_{-47}	0.86 ± 0.13	0.90	4B 5606	K06
8	960917	POW	$1.97^{+0.19}_{-0.20}$	-	-	0.98 ± 0.11	1.01	4B 5606	K06
9	960921	BAND	$[-1.0]$	$-2.91^{+0.27}_{-0.56}$	126^{+13}_{-13}	2.36 ± 0.10	0.57	4B 5609	K06
9	960921	CPL (*)	$1.27^{+0.29}_{-0.33}$	-	130^{+16}_{-23}	2.35 ± 0.13	0.60	4B 5609	K06
10	961022	CPL	$0.68^{+1.01}_{-1.37}$	-	280^{+341}_{-63}	0.63 ± 0.11	0.97	4B 5642	
10	961022	POW (*)	$1.80^{+0.22}_{-0.22}$	-	-	0.71 ± 0.08	0.92	4B 5642	
11	961208A	POW (*)	$1.92^{+0.37}_{-0.37}$	-	-	0.62 ± 0.11	0.36	G	
12	961228	CPL (*)	$-0.76^{+1.85}_{-3.48}$	-	165^{+41}_{-35}	0.74 ± 0.17	0.81	4B 5729	
12	961228	POW	$2.18^{+0.29}_{-0.29}$	-	-	0.89 ± 0.17	1.13	4B 5729	
13	970111	BAND	$-0.93^{+0.12}_{-0.11}$	$-3.40^{+0.40}_{-6.00}$	159^{+6}_{-6}	4.50 ± 0.09	0.85	W	
13	970111	CPL (*)	$0.98^{+0.10}_{-0.10}$	-	162^{+5}_{-5}	4.48 ± 0.09	0.86	W	
14	970116[a]	-	-	-	-	-	-	-	-
15	970117B	BAND	$-0.16^{+0.64}_{-0.43}$	$[-2.3]$	224^{+43}_{-31}	2.32 ± 0.08	0.84	G	
15	970117B	CPL (*)	$0.59^{+0.23}_{-0.25}$	-	279^{+30}_{-23}	2.34 ± 0.10	0.85	G	
16	970122	CPL (*)	$0.91^{+0.77}_{-1.02}$	-	155^{+68}_{-36}	0.58 ± 0.10	0.99	G	
17	970203	CPL (*)	$0.94^{+0.46}_{-0.56}$	-	205^{+51}_{-31}	0.89 ± 0.09	0.65	G	
18	970228	CPL (*)	$0.51^{+0.67}_{-0.86}$	-	157^{+24}_{-19}	0.65 ± 0.08	0.88	W	
19	970307	CPL (*)	$1.14^{+0.50}_{-0.65}$	-	128^{+24}_{-30}	1.01 ± 0.10	0.65	G	
20	970313	POW (*)	$1.88^{+0.18}_{-0.18}$	-	-	1.50 ± 0.13	0.96	G	
21	970315A	BAND	$-0.40^{+0.67}_{-0.47}$	$[-2.3]$	348^{+89}_{-59}	3.75 ± 0.17	0.95	4B 6124	K06
21	970315A	CPL (*)	$0.49^{+0.37}_{-0.39}$	-	378^{+64}_{-39}	3.80 ± 0.15	0.95	4B 6124	K06
22	970315B[a]	-	-	-	-	-	-	-	-
23	970402	POW (*)	$1.78^{+0.14}_{-0.13}$	-	-	0.86 ± 0.08	1.14	W	
23	970402	CPL	$1.00^{+0.43}_{-0.49}$	-	212^{+79}_{-35}	0.67 ± 0.07	0.93	W	
24	970420	BAND	$-0.64^{+0.50}_{-0.44}$	$-2.35^{+0.14}_{-0.37}$	214^{+39}_{-24}	4.60 ± 0.15	0.72	4B 6198	K06; only unit 4 used
24	970420	CPL (*)	$1.12^{+0.17}_{-0.18}$	-	263^{+18}_{-15}	4.74 ± 0.13	0.74	4B 6198	K06; only unit 4 used
25	970429	CPL (*)	$0.88^{+0.81}_{-0.86}$	-	177^{+57}_{-50}	0.69 ± 0.10	0.73	4B 6214	
26	970509	POW (*)	$2.05^{+0.25}_{-0.26}$	-	-	1.02 ± 0.14	0.60	4B 6226	
27	970517B	CPL (*)	$1.08^{+0.34}_{-0.38}$	-	382^{+254}_{-78}	1.23 ± 0.07	0.71	4B 6235	K06
27	970517B	BAND	$-1.10^{+0.51}_{-0.33}$	$[-2.3]$	381^{+159}_{-86}	1.23 ± 0.07	0.71	4B 6235	K06
28	970601[a]	-	-	-	-	-	-	-	-
29	970603	POW (*)	$1.61^{+0.29}_{-0.29}$	-	-	0.82 ± 0.11	0.84	4B 6249	K06
29	970603	CPL	$0.92^{+0.93}_{-1.80}$	-	>291	0.78 ± 0.13	0.84	4B 6249	K06
30	970612B[a]	-	-	-	-	-	-	-	-
31	970616	BAND	$[-1.0]$	< -2.25	206^{+31}_{-24}	2.83 ± 0.11	0.90	4B 6274	K06
31	970616	CPL (*)	$0.94^{+0.29}_{-0.33}$	-	224^{+21}_{-17}	2.78 ± 0.14	0.91	4B 6274	K06
32	970624A	POW (*)	$1.97^{+0.73}_{-0.67}$	-	-	0.68 ± 0.27	1.05	-	bad spectra
33	970624B	POW (*)	$2.11^{+0.17}_{-0.17}$	-	-	1.21 ± 0.10	0.77	-	
34	970625B	BAND	$-0.88^{+0.20}_{-0.18}$	$[-2.3]$	286^{+19}_{-17}	7.89 ± 0.17	0.81	-	only unit 4 used
34	970625B	CPL (*)	$0.97^{+0.12}_{-0.12}$	-	315^{+11}_{-10}	7.97 ± 0.14	0.71	-	only unit 4 used
35	970627A[a]	-	-	-	-	-	-	-	-
36	970627B[a]	-	-	-	-	-	-	-	-
37	970704[a]	-	-	-	-	-	-	-	-
38	970706	BAND	$-0.52^{+0.93}_{-0.46}$	$-2.46^{+0.17}_{-0.25}$	168^{+18}_{-22}	2.54 ± 0.11	0.85	-	
38	970706	CPL (*)	$1.17^{+0.18}_{-0.19}$	-	198^{+13}_{-12}	2.48 ± 0.19	0.94	-	
39	970715	CPL (*)	$1.43^{+0.37}_{-0.41}$	-	182^{+36}_{-71}	2.78 ± 0.21	1.17	-	
40	970815[a]	-	-	-	-	-	-	-	-
41	970816	CPL (*)	$1.03^{+0.24}_{-0.26}$	-	> 489	1.62 ± 0.06	0.67	4B 6336	
41	970816	POW	$1.40^{+0.06}_{-0.07}$	-	-	1.65 ± 0.06	0.70	4B 6336	K06
42	970827B	CPL (*)	$-0.32^{+0.88}_{-1.09}$	-	359^{+138}_{-60}	1.25 ± 0.14	0.72	4B 6349	

Table 2. continued.

# GRB	GRB	model	α	β	E_p	$\Phi(40-700)$	χ^2/dof	CAT	comment
-	-	-	-	-	(keV)	$(10^{-5}$ erg cm$^{-2})$	-	-	-
43	970831	BAND	$0.63^{+1.78}_{-0.87}$	$-2.48^{+0.14}_{-0.22}$	130^{+19}_{-19}	3.00 ± 0.09	0.93	4B 6353	K06
43	970831	CPL (*)	$0.82^{+0.20}_{-0.20}$	-	172^{+8}_{-8}	2.94 ± 0.10	1.06	4B 6353	K06
44	970919B	POW (*)	$2.77^{+0.25}_{-0.24}$	-	-	3.10 ± 0.40	0.61	4B 6389	K06
45	970922A	POW (*)	$2.72^{+0.33}_{-0.31}$	-	-	0.81 ± 0.12	0.47	-	
46	971019	CPL (*)	$1.29^{+0.38}_{-0.41}$	-	125^{+21}_{-30}	1.13 ± 0.09	0.75	G	
47	971022A	CPL (*)	$0.29^{+0.66}_{-0.86}$	-	342^{+127}_{-66}	0.90 ± 0.09	0.86	G	
48	971027A	CPL (*)	$1.12^{+0.56}_{-0.78}$	-	154^{+39}_{-34}	0.79 ± 0.09	0.90	K	
49	971029	BAND	$-0.81^{+0.58}_{-0.38}$	$-2.78^{+0.17}_{-0.27}$	137^{+8}_{-8}	3.68 ± 0.12	0.62	4B 6453	K06; only unit 3 used
49	971029	CPL (*)	$1.34^{+0.17}_{-0.18}$	-	136^{+11}_{-14}	3.76 ± 0.12	0.73	4B 6453	K06; only unit 3 used
50	971110	BAND	$-0.78^{+0.10}_{-0.09}$	[−2.3]	288^{+15}_{-14}	11.80 ± 0.13	1.11	4B 6472	K06
50	971110	CPL (*)	$0.87^{+0.06}_{-0.07}$	-	317^{+11}_{-10}	11.90 ± 0.13	1.07	4B 6472	K06
51	971114	POW (*)	$2.09^{+0.12}_{-0.10}$	-	-	1.66 ± 0.10	0.78	G	
52	971122	POW (*)	$1.63^{+0.11}_{-0.11}$	-	-	0.86 ± 0.06	0.72	4B 6492	
53	971127	CPL	$1.24^{+0.55}_{-0.68}$	-	228^{+249}_{-56}	0.61 ± 0.07	1.11	4B 6504	
53	971127	POW (*)	$1.87^{+0.15}_{-0.15}$	-	-	0.66 ± 0.06	1.15	4B 6504	
54	971206B	POW (*)	$2.10^{+0.24}_{-0.23}$	-	-	0.47 ± 0.07	0.66	W	
55	971208A	POW (*)	$2.00^{+0.21}_{-0.21}$	-	-	1.15 ± 0.13	0.73	G	
56	971208B	BAND	$0.89^{+1.55}_{-1.00}$	$-2.70^{+0.17}_{-0.29}$	125^{+16}_{-14}	8.82 ± 0.34	0.74	4B 6526	K06
56	971208B	CPL (*)	$0.71^{+0.26}_{-0.29}$	-	159^{+10}_{-9}	8.81 ± 0.38	0.86	4B 6526	K06
57	971214B	CPL (*)	$0.59^{+0.55}_{-0.69}$	-	208^{+54}_{-31}	0.66 ± 0.08	0.70	W	
58	971220	POW (*)	$1.29^{+0.16}_{-0.18}$	-	-	0.88 ± 0.08	0.79	4B 6539	K06
59	971223C	BAND	[−1.0]	< −2.25	186^{+37}_{-30}	1.54 ± 0.09	0.99	G	
59	971223C	CPL (*)	$0.95^{+0.51}_{-0.54}$	-	202^{+29}_{-26}	1.51 ± 0.13	1.00	G	
60	980105	CPL (*)	$0.38^{+0.85}_{-1.28}$	-	198^{+57}_{-31}	0.67 ± 0.10	0.54	4B 6560	K06
61	980124A[b]	-	-	-	-	-	-	-	
62	980127	CPL (*)	$0.37^{+0.49}_{-0.59}$	-	263^{+67}_{-40}	0.78 ± 0.08	0.76	G	
63	980203B	BAND	$-0.50^{+0.14}_{-0.10}$	[−2.3]	285^{+10}_{-11}	8.23 ± 0.09	1.58	4B 6587	K06
63	980203B	CPL (*)	$0.70^{+0.07}_{-0.06}$	-	326^{+8}_{-6}	8.38 ± 0.08	1.54	4B 6587	K06
64	980208B[a]	-	-	-	-	-	-	-	
65	980306B	BAND	[−1.0]	$-1.92^{+0.13}_{-0.24}$	249^{+49}_{-45}	4.02 ± 0.13	1.10	4B 6629	K06
65	980306B	CPL (*)	$1.27^{+0.18}_{-0.19}$	-	378^{+116}_{-57}	4.07 ± 0.12	1.12	4B 6629	K06
66	980306C	BAND	$-1.18^{+0.40}_{-0.29}$	[−2.3]	258^{+95}_{-54}	1.73 ± 0.08	0.77	4B 6630	K06
66	980306C	CPL (*)	$1.27^{+0.20}_{-0.20}$	-	288^{+75}_{-40}	1.74 ± 0.08	0.77	4B 6630	K06
67	980315B	CPL (*)	$0.91^{+0.62}_{-0.77}$	-	246^{+80}_{-42}	1.14 ± 0.12	0.53	4B 6642	K06
67	980315B	POW	$1.88^{+0.14}_{-0.14}$	-	-	1.27 ± 0.09	0.67	4B 6642	K06
68	980321	POW (*)	$2.50^{+0.28}_{-0.26}$	-	-	0.49 ± 0.08	0.87	4B 6651	
69	980329A	BAND	$-1.13^{+0.13}_{-0.12}$	[−2.3]	269^{+30}_{-25}	4.16 ± 0.08	0.79	W	
69	980329A	CPL (*)	$1.18^{+0.09}_{-0.10}$	-	291^{+25}_{-20}	4.17 ± 0.09	0.78	W	
70	980403[b]	-	-	-	-	-	-	-	
71	980420	CPL (*)	$0.50^{+0.60}_{-0.74}$	-	411^{+258}_{-80}	1.31 ± 0.10	0.84	4B 6694	K06
71	980420	BAND	$-0.35^{+1.56}_{-0.73}$	[−2.3]	368^{+266}_{-120}	1.28 ± 0.10	0.83	4B 6694	K06
72	980428	CPL	$0.96^{+0.62}_{-0.74}$	-	314^{+334}_{-68}	1.15 ± 0.12	0.88	-	
72	980428	POW (*)	$1.73^{+0.15}_{-0.14}$	-	-	1.26 ± 0.09	0.94	-	
73	980516	BAND	[−1.0]	$-1.80^{+0.08}_{-0.13}$	472^{+32}_{-31}	18.80 ± 0.10	1.18	G	only unit 1 used
73	980516	CPL (*)	$1.17^{+0.06}_{-0.06}$	-	> 584	19.10 ± 0.20	1.14	G	only unit 1 used
74	980519A	CPL (*)	$0.55^{+0.70}_{-0.84}$	-	279^{+85}_{-41}	0.64 ± 0.07	0.69	-	systematic deviations
75	980519B	CPL (*)	$0.68^{+0.54}_{-0.66}$	-	178^{+38}_{-25}	0.89 ± 0.10	0.59	W	
76	980615B	BAND	$-0.98^{+0.24}_{-0.19}$	$-2.48^{+0.14}_{-0.31}$	168^{+17}_{-15}	10.60 ± 0.20	1.05	G	deviations below 75 keV
76	980615B	CPL (*)	$1.23^{+0.08}_{-0.08}$	-	192^{+7}_{-7}	10.60 ± 0.20	1.09	G	deviations below 75 keV
77	980617	BAND	[−1.0]	$-2.43^{+0.27}_{-0.55}$	130^{+26}_{-25}	1.70 ± 0.14	1.03	4B 6829	
77	980617	CPL (*)	$1.24^{+0.41}_{-0.50}$	-	153^{+38}_{-25}	1.64 ± 0.16	1.09	4B 6829	
78	980624[a]	-	-	-	-	-	-	-	
79	980706B	POW (*)	$0.71^{+0.16}_{-0.17}$	-	-	0.85 ± 0.07	0.79	C	
80	980706D	BAND	$-1.35^{+0.22}_{-0.18}$	[−2.3]	344^{+101}_{-58}	3.56 ± 0.12	0.79	G	
80	980706D	CPL (*)	$1.31^{+0.18}_{-0.17}$	-	337^{+58}_{-41}	3.55 ± 0.11	0.78	G	
81	980709B	CPL (*)	$0.43^{+0.62}_{-0.69}$	-	224^{+36}_{-24}	1.22 ± 0.12	0.80	-	
82	980726[a]	-	-	-	-	-	-	-	
83	980728	BAND	$-0.61^{+1.01}_{-0.62}$	[−2.3]	204^{+77}_{-42}	1.28 ± 0.09	0.75	G	
83	980728	CPL (*)	$0.82^{+0.41}_{-0.48}$	-	237^{+53}_{-33}	1.26 ± 0.10	0.74	G	
84	980805[b]	-	-	-	-	-	-	-	
85	980808	POW (*)	$1.86^{+0.18}_{-0.18}$	-	-	1.57 ± 0.18	0.56	4B 6975	
86	980810B	BAND	$0.58^{+0.70}_{-0.53}$	$-2.31^{+0.16}_{-0.26}$	268^{+35}_{-29}	4.75 ± 0.12	0.86	4B 6985	K06
86	980810B	CPL (*)	$0.23^{+0.21}_{-0.22}$	-	338^{+18}_{-15}	4.96 ± 0.12	0.86	4B 6985	K06
87	980827C	BAND	$-1.25^{+0.90}_{-0.58}$	< −2.27	202^{+40}_{-58}	13.30 ± 1.00	0.83	-	only unit 3 used
87	980827C	CPL (*)	$1.52^{+0.36}_{-0.39}$	-	211^{+36}_{-89}	13.70 ± 0.80	0.83	-	only unit 3 used
88	981002	POW (*)	$1.39^{+0.27}_{-0.28}$	-	-	0.64 ± 0.09	1.11	S	

Table 2. continued.

# GRB	GRB	model	α	β	$E_{\rm p}$ (keV)	$\Phi(40-700)$ $(10^{-5}$ erg cm$^{-2})$	χ^2/dof	CAT	comment
-	-	-	-	-	(keV)	$(10^{-5}$ erg cm$^{-2})$	-	-	-
89	981018	cpl (*)	$0.79^{+1.02}_{-1.50}$	-	128^{+43}_{-56}	0.53 ± 0.10	1.19	S	
90	981107[(a)]	-	-	-	-	-	-	-	
91	981111	band	$-0.90^{+0.17}_{-0.14}$	[−2.3]	376^{+53}_{-41}	3.92 ± 0.09	0.91	G	
91	981111	cpl (*)	$0.90^{+0.13}_{-0.12}$	-	387^{+40}_{-29}	3.94 ± 0.08	0.90	G	
92	981125A	pow (*)	$2.10^{+0.17}_{-0.17}$	-	-	0.65 ± 0.06	1.08	4B 7228	
93	981125B	cpl	$0.85^{+0.67}_{-0.87}$	-	259^{+266}_{-64}	0.57 ± 0.09	0.72	4B 7230	
93	981125B	pow (*)	$1.69^{+0.17}_{-0.17}$	-	-	0.64 ± 0.07	0.82	4B 7230	
94	981203A	band	$-0.38^{+3.61}_{-0.63}$	$-1.76^{+0.18}_{-0.23}$	265^{+195}_{-148}	4.79 ± 0.22	1.05	4B 7247	only unit 3 used
94	981203A	cpl (*)	$0.98^{+0.27}_{-0.28}$	-	> 401	4.92 ± 0.20	1.07	4B 7247	only unit 3 used
95	981203B	band	$-0.22^{+1.01}_{-0.76}$	[−2.3]	286^{+167}_{-59}	1.53 ± 0.13	1.16	4B 7248	K06
95	981203B	cpl (*)	$0.56^{+0.54}_{-0.65}$	-	339^{+191}_{-63}	1.55 ± 0.14	1.18	4B 7248	K06
96	990117B	cpl (*)	$0.07^{+1.05}_{-1.68}$	-	203^{+94}_{-38}	0.57 ± 0.11	0.69	G	
97	990118A	cpl (*)	$-0.62^{+0.68}_{-0.81}$	-	206^{+14}_{-13}	1.55 ± 0.12	1.34	-	
98	990123A	band	$-0.84^{+0.04}_{-0.04}$	[−2.3]	552^{+27}_{-24}	17.10 ± 0.10	1.03	W	
98	990123A	cpl (*)	$0.84^{+0.04}_{-0.04}$	-	555^{+26}_{-23}	17.10 ± 0.10	1.03	W	
99	990128	band	$-0.64^{+0.66}_{-0.44}$	[−2.3]	152^{+20}_{-11}	1.96 ± 0.24	1.04	S	
99	990128	cpl (*)	$1.04^{+0.21}_{-0.22}$	-	187^{+14}_{-13}	1.82 ± 0.32	1.00	S	
100	990131	pow (*)	$2.36^{+0.16}_{-0.15}$	-	-	1.02 ± 0.09	0.87	G	
101	990226	cpl (*)	$0.00^{+0.46}_{-0.47}$	-	234^{+28}_{-21}	0.88 ± 0.07	0.59	4B 7429	
102	990403A	cpl (*)	$1.42^{+0.43}_{-0.52}$	-	144^{+37}_{-46}	0.76 ± 0.07	0.50	4B 7502	
102	990403A	pow	$2.08^{+0.11}_{-0.11}$	-	-	0.82 ± 0.05	0.59	4B 7502	
103	990506A	band	$-0.43^{+0.16}_{-0.18}$	[−2.3]	272^{+19}_{-16}	10.50 ± 0.20	1.20	P	
103	990506A	cpl (*)	$0.69^{+0.10}_{-0.11}$	-	320^{+13}_{-11}	10.70 ± 0.20	1.18	P	
104	990510	band	$-0.78^{+0.78}_{-0.49}$	< -2.27	153^{+29}_{-26}	1.65 ± 0.12	0.80	W	
104	990510	cpl (*)	$1.06^{+0.34}_{-0.39}$	-	169^{+26}_{-19}	1.63 ± 0.12	0.81	W	
105	990518B	band	$-0.55^{+0.10}_{-0.08}$	[−2.3]	411^{+25}_{-23}	9.77 ± 0.12	1.04	4B 7575	K06
105	990518B	cpl (*)	$0.59^{+0.08}_{-0.08}$	-	430^{+20}_{-18}	9.86 ± 0.11	1.04	4B 7575	K06
106	990521	band	$0.34^{+2.16}_{-1.13}$	[−2.3]	328^{+172}_{-83}	1.10 ± 0.12	0.78	G	
106	990521	cpl (*)	$-0.03^{+0.83}_{-1.01}$	-	374^{+127}_{-59}	1.13 ± 0.11	0.78	G	
107	990610	pow (*)	$1.61^{+0.20}_{-0.19}$	-	-	0.73 ± 0.07	0.79	-	
108	990620	pow (*)	$1.51^{+0.13}_{-0.14}$	-	-	2.14 ± 0.15	0.82	G	
109	990705	band	$-0.31^{+0.12}_{-0.12}$	[−2.3]	276^{+15}_{-13}	6.68 ± 0.09	0.90	W	
109	990705	cpl (*)	$0.51^{+0.07}_{-0.08}$	-	317^{+11}_{-10}	6.75 ± 0.10	0.89	W	
110	990712A	pow (*)	$1.56^{+0.18}_{-0.18}$	-	-	1.16 ± 0.11	0.88	4B 7647	
111	990712B	cpl	$1.26^{+0.65}_{-0.89}$	-	137^{+58}_{-69}	0.50 ± 0.08	0.66	W	
111	990712B	pow (*)	$2.05^{+0.17}_{-0.16}$	-	-	0.60 ± 0.08	0.77	W	
112	990718	cpl (*)	$1.00^{+0.45}_{-0.53}$	-	232^{+45}_{-34}	1.89 ± 0.16	0.88	4B 7660	K06; only unit 4 used
113	990720B	cpl (*)	$0.34^{+0.63}_{-0.78}$	-	148^{+20}_{-15}	0.62 ± 0.06	0.72	G	
114	990726	cpl	$1.30^{+0.50}_{-0.62}$	-	204^{+207}_{-54}	0.81 ± 0.11	0.94	G	
114	990726	pow (*)	$1.88^{+0.15}_{-0.15}$	-	-	0.86 ± 0.05	1.01	G	
115	990907	pow (*)	$1.88^{+0.15}_{-0.15}$	-	-	0.91 ± 0.08	0.79	W	
116	990913A	band	$-0.96^{+0.35}_{-0.28}$	[−2.3]	340^{+93}_{-59}	2.26 ± 0.09	0.61	G	
116	990913A	cpl (*)	$0.96^{+0.25}_{-0.26}$	-	351^{+71}_{-40}	2.26 ± 0.09	0.60	G	
117	991104	cpl (*)	$0.08^{+0.79}_{-1.12}$	-	222^{+46}_{-32}	0.55 ± 0.07	0.77	4B 7840	
118	991108	cpl	$0.63^{+0.56}_{-0.67}$	-	> 314	0.71 ± 0.07	0.90	4B 7845	
118	991108	pow (*)	$1.39^{+0.14}_{-0.14}$	-	-	0.74 ± 0.06	0.99	4B 7845	
119	991116	band	$-0.60^{+0.33}_{-0.28}$	[−2.3]	253^{+46}_{-32}	3.82 ± 0.14	0.76	G	
119	991116	cpl (*)	$0.81^{+0.17}_{-0.18}$	-	298^{+35}_{-26}	3.86 ± 0.14	0.76	G	
120	991120	pow (*)	$2.13^{+0.25}_{-0.25}$	-	-	0.60 ± 0.07	0.85	4B 7864	
121	991122A	pow (*)	$2.33^{+0.32}_{-0.31}$	-	-	0.70 ± 0.12	0.90	-	
122	991124B	pow (*)	$2.70^{+0.14}_{-0.13}$	-	-	2.30 ± 0.18	0.77	-	
123	991205C	cpl (*)	$0.74^{+0.80}_{-1.06}$	-	182^{+67}_{-42}	0.45 ± 0.08	0.75	S	
124	991216B	band	$-1.21^{+0.15}_{-0.13}$	< -2.02	324^{+60}_{-46}	13.10 ± 0.20	0.86	P	
124	991216B	cpl (*)	$1.30^{+0.06}_{-0.06}$	-	371^{+19}_{-16}	13.20 ± 0.10	0.86	P	
125	991221	pow (*)	$1.52^{+0.12}_{-0.12}$	-	-	1.45 ± 0.08	1.01	-	
126	991226A	pow (*)	$1.04^{+0.37}_{-0.42}$	-	-	1.93 ± 0.31	0.79	-	
127	000104A	cpl (*)	$1.09^{+0.42}_{-0.48}$	-	295^{+242}_{-66}	0.67 ± 0.06	0.73	4B 7933	
127	000104A	pow	$1.68^{+0.11}_{-0.11}$	-	-	0.72 ± 0.05	0.83	4B 7933	
128	000107C	cpl (*)	$1.29^{+0.66}_{-0.89}$	-	119^{+35}_{-88}	0.76 ± 0.10	0.67	4B 7938	K06
129	000109	band	$-1.10^{+0.08}_{-0.08}$	[−2.3]	580^{+99}_{-68}	9.12 ± 0.14	1.22	4B 7941	only unit 2, syst. deviat.
129	000109	cpl (*)	$1.10^{+0.08}_{-0.08}$	-	580^{+98}_{-66}	9.12 ± 0.14	1.22	4B 7941	only unit 2, syst. deviat.
130	000110	cpl (*)	$0.24^{+1.04}_{-1.51}$	-	245^{+160}_{-55}	0.37 ± 0.08	0.72	G	
131	000115	band	$-0.26^{+0.62}_{-0.43}$	$-2.79^{+0.29}_{-0.89}$	214^{+25}_{-21}	2.39 ± 0.10	0.94	4B 7954	K06
131	000115	cpl (*)	$0.66^{+0.26}_{-0.28}$	-	238^{+15}_{-13}	2.45 ± 0.09	0.95	4B 7954	K06
132	000119B	cpl (*)	$0.52^{+0.58}_{-0.72}$	-	262^{+84}_{-45}	0.65 ± 0.08	0.87	G	

Table 2. continued.

# GRB	GRB	model	α	β	E_p (keV)	$\Phi(40-700)$ (10^{-5} erg cm^{-2})	χ^2/dof	CAT	comment
-	-	-	-	-	(keV)	(10^{-5} erg cm^{-2})	-	-	-
133	000210	BAND	$-1.02^{+0.08}_{-0.08}$	[−2.3]	525^{+74}_{-54}	4.48 ± 0.07	0.71	W	
133	000210	CPL (*)	$1.02^{+0.08}_{-0.08}$	-	527^{+71}_{-51}	4.49 ± 0.07	0.71	W	
134	000214A	CPL (*)	$0.50^{+0.34}_{-0.39}$	-	271^{+50}_{-33}	0.94 ± 0.07	0.60	W	
135	000218A	POW (*)	$2.49^{+0.18}_{-0.11}$	-	-	1.86 ± 0.17	1.02	-	
136	000218B	POW (*)	$1.29^{+0.11}_{-0.11}$	-	-	1.41 ± 0.08	0.74	-	
137	000226	BAND	$-0.77^{+0.12}_{-0.11}$	[−2.3]	301^{+20}_{-18}	9.15 ± 0.12	1.09	G	
137	000226	CPL (*)	$0.81^{+0.08}_{-0.08}$	-	324^{+14}_{-12}	9.21 ± 0.11	1.04	G	
138	000227	CPL	$1.46^{+0.47}_{-0.52}$	-	184^{+97}_{-87}	1.39 ± 0.14	0.97	4B 8001	
138	000227	POW (*)	$2.00^{+0.14}_{-0.13}$	-	-	1.48 ± 0.12	1.02	4B 8001	
139	000301C	CPL (*)	$0.79^{+0.39}_{-0.45}$	-	185^{+23}_{-19}	1.32 ± 0.10	0.76	G	
140	000312	CPL (*)	$0.70^{+0.66}_{-0.87}$	-	169^{+35}_{-25}	0.81 ± 0.10	0.96	4B 8030	
141	000323	CPL (*)	$0.75^{+0.40}_{-0.44}$	-	170^{+21}_{-15}	1.08 ± 0.08	0.91	I	
142	000327	CPL (*)	$0.90^{+0.41}_{-0.48}$	-	222^{+45}_{-33}	1.16 ± 0.10	0.89	G	
143	000328	POW (*)	$2.41^{+0.17}_{-0.17}$	-	-	1.48 ± 0.13	1.43	-	
144	000419	CPL (*)	$0.80^{+0.33}_{-0.35}$	-	241^{+46}_{-27}	1.10 ± 0.08	0.60	I	
145	000420B	POW (*)	$2.48^{+0.20}_{-0.20}$	-	-	2.22 ± 0.30	1.32	4B 8081	K06
145	000420B	CPL	$0.70^{+1.14}_{-1.58}$	-	174^{+42}_{-118}	1.65 ± 0.33	1.19	4B 8081	K06
146	000421	CPL (*)	$-0.35^{+1.54}_{-2.47}$	-	152^{+26}_{-42}	1.12 ± 0.24	1.23	4B 8084	
147	000429	BAND	$-0.92^{+0.30}_{-0.26}$	[−2.3]	381^{+114}_{-54}	2.09 ± 0.10	0.77	I	
147	000429	CPL (*)	$0.90^{+0.25}_{-0.25}$	-	384^{+101}_{-55}	2.10 ± 0.09	0.76	I	
148	000523	CPL (*)	$-0.53^{+0.88}_{-0.80}$	-	252^{+32}_{-26}	1.18 ± 0.13	1.11	-	
149	000528	CPL (*)	$0.68^{+0.36}_{-0.41}$	-	140^{+12}_{-10}	1.43 ± 0.09	0.67	W	
150	000615B	POW (*)	$1.66^{+0.28}_{-0.28}$	-	-	1.63 ± 0.26	0.79	I	
151	000621	CPL (*)	$-0.29^{+0.91}_{-1.11}$	-	256^{+28}_{-25}	1.21 ± 0.14	0.84	G	
152	000630	BAND	$-0.67^{+0.91}_{-0.38}$	< -2.18	216^{+42}_{-56}	1.41 ± 0.07	0.79	I	
152	000630	CPL (*)	$1.07^{+0.25}_{-0.28}$	-	234^{+28}_{-21}	1.42 ± 0.07	0.78	I	
153	000718B	BAND	$-0.97^{+0.10}_{-0.09}$	[−2.3]	409^{+46}_{-38}	6.80 ± 0.13	1.13	G	
153	000718B	CPL (*)	$0.95^{+0.09}_{-0.09}$	-	406^{+39}_{-31}	6.81 ± 0.13	1.11	G	
154	000727	POW (*)	$1.94^{+0.12}_{-0.12}$	-	-	1.47 ± 0.09	0.78	I	
155	000811	BAND	$-1.03^{+0.54}_{-0.39}$	[−2.3]	216^{+53}_{-34}	3.08 ± 0.12	0.94	I	
155	000811	CPL (*)	$1.25^{+0.21}_{-0.23}$	-	257^{+34}_{-25}	3.11 ± 0.12	0.93	I	
156	000904	CPL	$0.91^{+1.02}_{-1.32}$	-	242^{+83}_{-176}	0.67 ± 0.12	0.79	G	
156	000904	POW (*)	$2.08^{+0.22}_{-0.21}$	-	-	0.78 ± 0.10	0.82	G	
157	000906	CPL (*)	$-0.17^{+0.90}_{-1.07}$	-	162^{+32}_{-17}	0.53 ± 0.07	0.51	G	
158	001004	BAND	$0.91^{+2.35}_{-1.25}$	$-2.13^{+0.15}_{-0.24}$	187^{+72}_{-40}	3.80 ± 0.20	1.05	I	
158	001004	CPL (*)	$0.62^{+0.28}_{-0.31}$	-	304^{+34}_{-25}	4.02 ± 0.15	1.07	I	
159	001011C	BAND	[−1.0]	< -1.79	345^{+57}_{-53}	1.90 ± 0.07	0.66	W	
159	001011C	CPL (*)	$1.10^{+0.17}_{-0.18}$	-	398^{+119}_{-63}	2.02 ± 0.07	0.66	W	
160	001013	BAND	[−1.0]	$-2.71^{+0.21}_{-0.42}$	102^{+12}_{-10}	2.73 ± 0.12	1.05	G	
160	001013	CPL (*)	$1.42^{+0.21}_{-0.23}$	-	106^{+13}_{-16}	2.68 ± 0.11	1.07	G	
161	001019	CPL (*)	$0.64^{+0.69}_{-0.87}$	-	201^{+48}_{-34}	0.78 ± 0.09	0.67	I	
162	001110	POW (*)	$1.82^{+0.14}_{-0.12}$	-	-	1.27 ± 0.10	1.16	G	
163	001115	BAND	$0.58^{+3.88}_{-1.56}$	[−2.3]	220^{+93}_{-50}	0.99 ± 0.13	0.68	G	
163	001115	CPL (*)	$0.10^{+0.94}_{-1.25}$	-	261^{+53}_{-37}	0.96 ± 0.14	0.62	G	
164	001206A	CPL (*)	$0.97^{+0.49}_{-0.61}$	-	252^{+166}_{-57}	0.73 ± 0.09	0.86	G	
164	001206A	POW	$1.70^{+0.13}_{-0.13}$	-	-	0.81 ± 0.07	0.99	G	
165	001206C	POW (*)	$1.67^{+0.24}_{-0.24}$	-	-	0.74 ± 0.10	1.14	G	
166	001212A	POW (*)	$1.61^{+0.13}_{-0.13}$	-	-	0.70 ± 0.05	0.92	G	
167	001212B	BAND	$-0.92^{+0.90}_{-0.58}$	[−2.3]	208^{+65}_{-37}	2.20 ± 0.13	0.72	I	
167	001212B	CPL (*)	$1.35^{+0.27}_{-0.29}$	-	264^{+49}_{-35}	2.26 ± 0.11	0.73	I	
168	001213	POW (*)	$2.36^{+0.51}_{-0.45}$	-	-	1.31 ± 0.32	2.18	-	noisy spectrum
168	001213	CPL	$-0.60^{+2.40}_{-4.07}$	-	152^{+53}_{-97}	1.01 ± 0.33	1.93	-	noisy spectrum
169	001217	POW (*)	$2.18^{+0.36}_{-0.34}$	-	-	0.33 ± 0.07	1.08	G	
170	001219A	POW (*)	$2.16^{+0.29}_{-0.28}$	-	-	1.54 ± 0.23	0.93	G	
171	001228	POW (*)	$1.87^{+0.03}_{-0.04}$	-	-	6.53 ± 0.13	1.55	-	anomaly spec.
172	010109	BAND	$-0.87^{+0.37}_{-0.28}$	[−2.3]	338^{+72}_{-50}	3.69 ± 0.14	0.79	I	only unit 2 used
172	010109	CPL (*)	$0.93^{+0.22}_{-0.23}$	-	363^{+51}_{-34}	3.73 ± 0.12	0.78	I	only unit 2 used
173	010119A	CPL (*)	$1.14^{+0.41}_{-0.47}$	-	217^{+40}_{-35}	1.40 ± 0.11	0.66	G	
174	010127	POW (*)	$1.65^{+0.13}_{-0.12}$	-	-	1.29 ± 0.08	0.94	-	
175	010213	CPL	$1.34^{+0.56}_{-0.74}$	-	136^{+49}_{-67}	0.53 ± 0.07	0.90	W	
175	010213	POW (*)	$2.07^{+0.15}_{-0.15}$	-	-	0.60 ± 0.05	1.01	W	
176	010222A	BAND	$-1.05^{+0.21}_{-0.16}$	$-2.14^{+0.13}_{-0.58}$	291^{+52}_{-43}	8.86 ± 0.13	1.01	W	
176	010222A	CPL (*)	$1.20^{+0.07}_{-0.07}$	-	344^{+21}_{-17}	8.97 ± 0.11	1.02	W	
177	010226A	CPL (*)	$-0.22^{+1.02}_{-1.39}$	-	151^{+22}_{-17}	0.61 ± 0.08	0.58	G	
178	010317	BAND	$-0.96^{+1.14}_{-0.53}$	[−2.3]	218^{+114}_{-94}	1.24 ± 0.09	0.60	G	

Table 2. continued.

# GRB	GRB	model	α	β	E_p (keV)	$\Phi(40-700)$ $(10^{-5}$ erg cm$^{-2})$	χ^2/dof	CAT	comment
-	-	-	-	-	-	-	-	-	-
178	010317	CPL (*)	$1.10^{+0.39}_{-0.42}$	-	251^{+82}_{-41}	1.24 ± 0.09	0.60	G	
179	010324	BAND	$0.28^{+1.93}_{-1.04}$	[−2.3]	149^{+38}_{-26}	1.71 ± 0.10	1.06	A	
179	010324	CPL (*)	$0.60^{+0.40}_{-0.46}$	-	196^{+26}_{-20}	1.63 ± 0.13	1.01	A	
180	010326	CPL	$0.96^{+0.80}_{-0.98}$	-	208^{+106}_{-58}	0.84 ± 0.13	0.67	I	
180	010326	POW (*)	$1.96^{+0.20}_{-0.21}$	-	-	0.91 ± 0.11	0.73	I	
181	010408B	BAND	$-1.04^{+0.69}_{-0.61}$	[−2.3]	147^{+32}_{-25}	1.60 ± 0.10	0.72	-	
181	010408B	CPL (*)	$1.44^{+0.17}_{-0.36}$	-	173^{+30}_{-27}	1.60 ± 0.09	0.71	-	
182	010412	BAND	$-0.70^{+0.22}_{-0.19}$	[−2.3]	216^{+20}_{-17}	2.96 ± 0.06	0.76	W	
182	010412	CPL (*)	$0.90^{+0.11}_{-0.12}$	-	253^{+15}_{-13}	2.95 ± 0.07	0.71	W	
183	010418	BAND	$-0.79^{+0.56}_{-0.47}$	< −1.75	270^{+200}_{-77}	1.88 ± 0.08	1.11	G	
183	010418	CPL (*)	$1.03^{+0.23}_{-0.25}$	-	368^{+108}_{-54}	1.90 ± 0.08	1.11	G	
184	010427B	BAND	$-0.95^{+0.10}_{-0.09}$	[−2.3]	606^{+75}_{-66}	5.61 ± 0.08	1.02	G	
184	010427B	CPL (*)	$0.95^{+0.10}_{-0.05}$	-	607^{+54}_{-65}	5.61 ± 0.08	1.02	G	
185	010504	BAND	$-1.24^{+0.24}_{-0.20}$	[−2.3]	404^{+184}_{-87}	1.96 ± 0.08	0.81	G	
185	010504	CPL (*)	$1.23^{+0.20}_{-0.22}$	-	405^{+169}_{-71}	1.97 ± 0.08	0.81	G	
186	010517	POW (*)	$1.61^{+0.26}_{-0.26}$	-	-	1.08 ± 0.14	0.60	-	
187	010521	POW (*)	$2.19^{+0.64}_{-0.56}$	-	-	1.18 ± 0.35	0.66	-	
188	010619	BAND	$-1.17^{+1.32}_{-0.53}$	[−2.3]	159^{+60}_{-42}	1.70 ± 0.12	1.06	G	
188	010619	CPL (*)	$1.09^{+0.42}_{-0.51}$	-	172^{+33}_{-27}	1.60 ± 0.14	1.00	G	
189	010710B	CPL (*)	$0.91^{+0.25}_{-0.26}$	-	175^{+11}_{-11}	2.29 ± 0.10	0.92	G	
190	010711	POW (*)	$2.49^{+0.25}_{-0.24}$	-	-	4.91 ± 0.68	1.08	-	
191	010715	POW (*)	$2.17^{+0.41}_{-0.41}$	-	-	0.90 ± 0.15	0.75	-	
192	010721	POW (*)	$0.81^{+0.23}_{-0.25}$	-	-	0.48 ± 0.05	0.95	G	
193	010801	BAND	$-0.63^{+0.32}_{-0.17}$	[−2.3]	227^{+19}_{-16}	4.35 ± 0.10	0.88	G	
193	010801	CPL (*)	$0.96^{+0.13}_{-0.14}$	-	272^{+13}_{-11}	4.41 ± 0.09	0.84	G	
194	010804	POW (*)	$2.55^{+0.19}_{-0.18}$	-	-	2.28 ± 0.23	0.89	-	
195	010813	CPL (*)	$0.46^{+0.57}_{-0.66}$	-	388^{+109}_{-53}	1.35 ± 0.10	0.78	-	
196	010818A	POW (*)	$1.62^{+0.13}_{-0.13}$	-	-	1.06 ± 0.75	0.74	G	
197	010826	BAND	$-0.73^{+0.32}_{-0.25}$	[−2.3]	288^{+54}_{-41}	3.10 ± 0.11	0.82	G	
197	010826	CPL (*)	$0.80^{+0.19}_{-0.20}$	-	313^{+39}_{-28}	3.10 ± 0.11	0.81	G	
198	010921	POW (*)	$2.39^{+0.12}_{-0.12}$	-	-	1.63 ± 0.11	0.81	I	
199	010922	CPL (*)	$0.41^{+0.45}_{-0.54}$	-	204^{+17}_{-15}	2.03 ± 0.13	0.84	-	
200	011003	BAND	$-0.70^{+0.39}_{-0.30}$	[−2.3]	288^{+44}_{-34}	2.34 ± 0.08	0.85	-	
200	011003	CPL (*)	$0.80^{+0.20}_{-0.20}$	-	319^{+27}_{-20}	2.36 ± 0.06	0.82	-	

(a) Unavailable data packets.
(b) Bad spectra.
(*) Best fit model for a given GRB.

Table 3. Spectral fitting results of the time-resolved spectra for each bright GRB that happened to be sampled by more 128-s time intervals. Spectral models are the same as in Table 2. Intervals are the same as in Table 1. Asterisks mark the best-fit model for the spectra that were fit with different models.

# GRB	GRB	Interval	model	α	β	E_p (keV)	$\Phi(40-700)$ (10^{-5} erg cm^{-2})	χ^2/dof	CAT	comment
-	-	-	-	-	-	(keV)	(10^{-5} erg cm^{-2})	-	-	-
1	960703	A	CPL	$0.89^{+0.43}_{-0.48}$	-	307^{+140}_{-56}	0.75 ± 0.06	0.84	4B 5526	
1	960703	B	POW	$2.04^{+0.19}_{-0.19}$	-	-	0.47 ± 0.05	1.29	4B 5526	
4	960805B	A	POW (*)	$2.08^{+0.20}_{-0.20}$	-	-	0.92 ± 0.11	1.03	-	
4	960805B	A	CPL	< 0.65	-	194^{+31}_{-25}	0.71 ± 0.13	0.68	-	
4	960805B	B	CPL	$0.33^{+0.44}_{-0.48}$	-	164^{+13}_{-14}	1.96 ± 0.15	0.85	-	
5	960806	A	POW	$1.96^{+3.03}_{-1.78}$	-	-	0.19 ± 0.10	1.36	4B 5566	
5	960806	B	CPL	$0.58^{+0.68}_{-0.85}$	-	231^{+56}_{-35}	1.11 ± 0.13	0.77	4B 5566	
6	960825	A	CPL	$0.33^{+0.39}_{-0.44}$	-	241^{+16}_{-15}	2.82 ± 0.15	0.58	G	
6	960825	B	CPL	$0.19^{+0.58}_{-0.69}$	-	254^{+27}_{-23}	1.85 ± 0.13	0.77	G	
7	960912	A	CPL	$1.04^{+0.46}_{-0.55}$	-	269^{+176}_{-57}	0.71 ± 0.07	0.68	4B 5601	
7	960912	B	POW	$2.75^{+0.88}_{-0.67}$	-	-	0.12 ± 0.05	0.74	4B 5601	
8	960917	A	POW	$1.92^{+0.28}_{-0.28}$	-	-	0.51 ± 0.08	0.64	4B 5606	
8	960917	B	POW	$2.07^{+0.29}_{-0.29}$	-	-	0.48 ± 0.08	0.91	4B 5606	
11	961208A	A	POW	$1.72^{+0.30}_{-0.32}$	-	-	0.49 ± 0.08	0.90	G	
11	961208A	B	POW	$2.58^{+1.75}_{-1.43}$	-	-	0.14 ± 0.08	0.29	G	
12	961228	A	POW	$2.17^{+0.21}_{-0.20}$	-	-	0.89 ± 0.12	1.14	4B 5729	
12	961228	A	CPL (*)	$-0.32^{+1.31}_{-1.96}$	-	165^{+31}_{-28}	0.75 ± 0.13	0.74	4B 5729	
12	961228$^{(a)}$	B	-	-	-	-	-	-	-	
15	970117B	A	CPL	$0.52^{+0.18}_{-0.19}$	-	291^{+22}_{-19}	2.30 ± 0.08	0.92	G	
15	970117B$^{(b)}$	B	-	-	-	-	-	>3	-	
23	970402	A	CPL	$1.01^{+0.42}_{-0.50}$	-	209^{+70}_{-35}	0.70 ± 0.07	0.72	W	
23	970402	B	POW	$1.62^{+1.76}_{-1.73}$	-	-	0.08 ± 0.06	0.68	W	
29	970603	A	POW	$1.34^{+0.29}_{-0.29}$	-	-	0.58 ± 0.08	0.67	4B 6249	
29	970603	B	POW	$2.26^{+0.81}_{-0.67}$	-	-	0.28 ± 0.10	0.65	4B 6249	
31	970616	A	POW	$1.61^{+1.11}_{-1.15}$	-	-	0.17 ± 0.07	0.52	4B 6274	
31	970616	B	CPL	$1.10^{+0.22}_{-0.24}$	-	243^{+22}_{-18}	2.57 ± 0.10	1.01	4B 6274	
31	970616	B	BAND (*)	$0.25^{+2.53}_{-0.94}$	$-2.26^{+0.14}_{-0.21}$	171^{+35}_{-35}	2.45 ± 0.11	0.93	4B 6274	
32	970624A	A	POW	$2.24^{+0.67}_{-0.75}$	-	-	0.59 ± 0.27	0.54	-	
32	970624A	B	POW	$1.32^{+2.63}_{-3.78}$	-	-	0.18 ± 0.16	0.94	-	
33	970624B	A	POW	$2.12^{+0.18}_{-0.17}$	-	-	0.82 ± 0.07	0.64	-	
33	970624B	B	POW	$2.11^{+0.37}_{-0.36}$	-	-	0.39 ± 0.07	0.46	-	
42	970827B	A	CPL	$0.06^{+0.90}_{-0.95}$	-	389^{+289}_{-80}	0.89 ± 0.10	0.51	4B 6349	
42	970827B	B	POW	$1.38^{+0.41}_{-0.43}$	-	-	0.41 ± 0.09	0.74	4B 6349	
43	970831	A	CPL (*)	$0.69^{+0.94}_{-1.36}$	-	147^{+42}_{-33}	0.41 ± 0.07	1.02	4B 6353	
43	970831	A	BAND	$[-1.0]$	< -2.13	139^{+46}_{-41}	0.44 ± 0.06	1.01	4B 6353	
43	970831	B	CPL	$0.82^{+0.16}_{-0.18}$	-	176^{+8}_{-7}	2.53 ± 0.07	0.98	4B 6353	
43	970831	B	BAND (*)	$0.85^{+0.88}_{-0.50}$	$-2.56^{+0.15}_{-0.21}$	143^{+14}_{-16}	2.56 ± 0.07	0.87	4B 6353	
47	971022A	A	CPL	$-0.28^{+0.68}_{-0.79}$	-	319^{+59}_{-39}	0.73 ± 0.07	0.89	G	
47	971022A	B	POW	$1.92^{+0.78}_{-0.73}$	-	-	0.16 ± 0.06	0.97	G	
48	971027A	A	CPL	$1.18^{+0.42}_{-0.39}$	-	167^{+35}_{-27}	0.79 ± 0.07	0.95	K	
48	971027A$^{(a)}$	B	-	-	-	-	-	-	-	
50	971110	A	CPL	$0.45^{+0.29}_{-0.37}$	-	201^{+17}_{-14}	1.35 ± 0.08	0.57	4B 6472	
50	971110	B	CPL	$0.83^{+0.09}_{-0.10}$	-	327^{+17}_{-15}	4.73 ± 0.08	0.80	4B 6472	
50	971110	C	CPL	$0.90^{+0.08}_{-0.08}$	-	345^{+17}_{-15}	5.76 ± 0.08	0.96	4B 6472	
51	971114	A	CPL	$1.32^{+0.34}_{-0.40}$	-	157^{+26}_{-29}	1.40 ± 0.10	0.64	G	
51	971114	B	POW	$2.86^{+1.80}_{-1.47}$	-	-	0.13 ± 0.07	0.77	G	
54	971206B	A	POW	$2.39^{+1.51}_{-1.06}$	-	-	0.08 ± 0.05	0.59	W	
54	971206B	B	POW	$2.05^{+0.20}_{-0.19}$	-	-	0.39 ± 0.05	0.63	W	
54	971206B	B	CPL (*)	$0.64^{+1.05}_{-1.47}$	-	138^{+44}_{-36}	0.32 ± 0.06	0.43	W	
56	971208B	A	POW (*)	$1.38^{+0.03}_{-0.03}$	-	-	0.67 ± 0.12	0.65	4B 6526	
56	971208B	A	CPL	$0.45^{+1.08}_{-1.57}$	-	> 282	0.67 ± 0.12	0.60	4B 6526	
56	971208B	B	CPL	$0.98^{+0.25}_{-0.28}$	-	184^{+16}_{-14}	3.18 ± 0.14	0.75	4B 6526	
56	971208B	B	BAND (*)	$0.40^{+1.49}_{-0.86}$	$-2.50^{+0.17}_{-0.24}$	135^{+21}_{-20}	3.14 ± 0.14	0.64	4B 6526	
56	971208B	C	CPL (*)	$0.71^{+0.45}_{-0.56}$	-	156^{+17}_{-15}	2.06 ± 0.15	0.69	4B 6526	
56	971208B	C	BAND	$[-1.0]$	$-2.85^{+0.41}_{-3.92}$	146^{+22}_{-20}	2.17 ± 0.12	0.66	4B 6526	
56	971208B	D	CPL	$0.16^{+0.70}_{-0.88}$	-	146^{+18}_{-16}	1.30 ± 0.13	0.75	4B 6526	
56	971208B	E	CPL	$0.65^{+1.00}_{-1.45}$	-	113^{+25}_{-44}	0.83 ± 0.13	0.49	4B 6526	
56	971208B	F	POW (*)	$2.29^{+0.32}_{-0.29}$	-	-	0.60 ± 0.12	0.73	4B 6526	
56	971208B	F	CPL	$0.37^{+1.55}_{-2.77}$	-	125^{+43}_{-98}	0.52 ± 0.13	0.44	4B 6526	
56	971208B	G	POW (*)	$2.49^{+0.44}_{-0.38}$	-	-	0.44 ± 0.11	1.09	4B 6526	
56	971208B	G	CPL	< 1.98	-	< 152	0.38 ± 0.11	0.74	4B 6526	
59	971223C	A	POW	$2.08^{+0.44}_{-0.21}$	-	-	0.30 ± 0.06	0.88	G	
59	971223C	B	CPL	$0.92^{+0.35}_{-0.41}$	-	202^{+24}_{-21}	1.24 ± 0.10	0.91	G	

Table 3. continued.

# GRB	GRB	Interval	model	α	β	$E_{\rm p}$ (keV)	$\Phi(40-700)$ $(10^{-5}$ erg cm$^{-2})$	χ^2/dof	CAT	comment
-	-	-	-	-	-			-	-	-
65	980306B	A	POW	$1.95^{+0.19}_{-0.19}$	-	-	0.63 ± 0.06	0.64	4B 6629	
65	980306B	B	CPL	$0.98^{+0.21}_{-0.23}$	-	391^{+90}_{-50}	2.19 ± 0.08	0.81	4B 6629	
65	980306B	C	CPL	$1.28^{+0.33}_{-0.37}$	-	287^{+158}_{-54}	1.22 ± 0.08	0.90	4B 6629	
68	980321	A	POW	> 1.13	-	-	0.07 ± 0.06	1.17	4B 6651	
68	980321	B	POW	$2.53^{+0.24}_{-0.22}$	-	-	0.44 ± 0.05	0.69	4B 6651	
72	980428	A	POW	$1.72^{+0.13}_{-0.13}$	-	-	1.01 ± 0.06	0.66	-	
72	980428	A	CPL	$0.93^{+0.57}_{-0.68}$	-	317^{+227}_{-62}	0.93 ± 0.09	0.57	-	
72	980428	B	POW (*)	$1.79^{+0.58}_{-0.55}$	-	-	0.25 ± 0.06	0.34	-	
75	980519B	A	CPL	$1.06^{+0.39}_{-0.46}$	-	177^{+41}_{-25}	0.82 ± 0.08	0.71	W	
75	980519B	B	POW	$1.72^{+0.81}_{-0.73}$	-	-	0.12 ± 0.06	1.45	W	
76	980615B	A	CPL (*)	$1.12^{+0.26}_{-0.29}$	-	372^{+167}_{-68}	2.07 ± 0.11	0.71	G	
76	980615B	A	BAND	$-1.13^{+0.34}_{-0.26}$	$[-2.3]$	372^{+190}_{-88}	2.07 ± 0.11	0.71	G	
76	980615B	B	CPL	$1.18^{+0.08}_{-0.08}$	-	168^{+5}_{-5}	8.46 ± 0.13	1.17	G	deviations belew 80 keV
76	980615B	B	BAND (*)	$-0.89^{+0.21}_{-0.17}$	$-2.63^{+0.13}_{-0.21}$	151^{+9}_{-9}	8.49 ± 0.13	1.09	G	deviations below 80 keV
77	980617	A	POW	> 0.10	-	-	0.09 ± 0.07	0.36	4B 6829	
77	980617	B	CPL	$1.28^{+0.28}_{-0.31}$	-	184^{+37}_{-26}	1.29 ± 0.09	0.84	4B 6829	
77	980617	C	POW (*)	$2.36^{+0.29}_{-0.27}$	-	-	0.35 ± 0.06	1.16	4B 6829	
77	980617	C	CPL	< 1.16	-	99^{+18}_{-22}	0.27 ± 0.05	0.81	4B 6829	
80	980706D	A	CPL	$1.01^{+0.17}_{-0.16}$	-	336^{+39}_{-27}	3.10 ± 0.08	0.87	G	
80	980706D	B	POW	$2.52^{+0.33}_{-0.31}$	-	-	0.45 ± 0.07	0.72	G	
81	980709B	A	CPL	$-0.02^{+0.51}_{-0.64}$	-	253^{+28}_{-21}	1.00 ± 0.08	0.81	-	
81	980709B	B	POW	$2.72^{+0.59}_{-0.51}$	-	-	0.30 ± 0.07	0.32	-	
83	980728	A	POW	$2.01^{+0.55}_{-0.50}$	-	-	0.18 ± 0.05	0.48	G	
83	980728	B	CPL	$0.80^{+0.34}_{-0.38}$	-	249^{+45}_{-29}	1.10 ± 0.07	0.69	G	
85	980808	A	POW	3.74^{+3}_{-3}	-	-	0.07 ± 0.04	0.70	4B 6975	
85	980808	B	POW (*)	$1.81^{+0.13}_{-0.13}$	-	-	1.49 ± 0.13	0.55	4B 6975	
85	980808	B	CPL	$1.29^{+0.44}_{-0.52}$	-	238^{+291}_{-62}	1.40 ± 0.16	0.46	4B 6975	
87	980827C	A	CPL (*)	$1.53^{+0.27}_{-0.28}$	-	213^{+28}_{-52}	13.44 ± 0.55	0.92	-	only unit 3 used
87	980827C	A	BAND	$-1.34^{+0.60}_{-0.45}$	< -2.31	205^{+35}_{-41}	13.20 ± 0.77	0.93	-	only unit 3 used
87	980827C	B	POW	3.30^{+3}_{-3}	-	-	0.34 ± 0.10	0.34	-	only unit 3 used
88	981002	A	POW	$1.24^{+0.24}_{-0.25}$	-	-	0.53 ± 0.07	0.85	S	
88	981002	B	POW	$1.95^{+1.56}_{-1.25}$	-	-	0.12 ± 0.07	1.26	S	
89	981018	A	POW (*)	$2.05^{+0.20}_{-0.20}$	-	-	0.50 ± 0.06	1.08	S	
89	981018	A	CPL	$0.91^{+0.96}_{-1.42}$	-	138^{+60}_{-60}	0.42 ± 0.08	0.96	S	
89	981018	B	POW	$2.41^{+0.83}_{-0.68}$	-	-	0.14 ± 0.05	0.68	S	
94	981203A	A	POW	< 2.14	-	-	0.13 ± 0.11	0.53	4B 7247	only unit 3 used
94	981203A	B	CPL	$0.93^{+0.19}_{-0.20}$	-	444^{+99}_{-56}	4.10 ± 0.12	0.98	4B 7247	only unit 3 used
94	981203A	C	POW (*)	$1.59^{+0.27}_{-0.29}$	-	-	0.66 ± 0.12	0.62	4B 7247	only unit 3 used
94	981203A	C	CPL	$0.97^{+0.85}_{-1.58}$	-	> 227	0.65 ± 0.12	0.61	4B 7247	only unit 3 used
95	981203B	A	CPL	$0.54^{+0.29}_{-0.32}$	-	320^{+49}_{-33}	1.44 ± 0.07	1.17	4B 7248	
95	981203B	B	POW	$1.41^{+0.38}_{-0.40}$	-	-	0.29 ± 0.06	0.78	4B 7248	
96	990117B	A	CPL	$0.05^{+0.65}_{-0.84}$	-	233^{+52}_{-34}	0.58 ± 0.07	0.67	G	
96	990117B$^{(b)}$	B	-	-	-	-	-	>2	-	
98	990123A	A	CPL	$0.70^{+0.05}_{-0.06}$	-	> 649	8.66 ± 0.08	0.89	W	
98	990123A	B	CPL	$0.90^{+0.05}_{-0.05}$	-	411^{+19}_{-17}	8.42 ± 0.08	0.90	W	
100	990131	A	POW	$2.68^{+0.41}_{-0.36}$	-	-	0.34 ± 0.06	0.54	G	
100	990131	B	CPL	$0.57^{+0.89}_{-1.22}$	-	117^{+21}_{-28}	0.57 ± 0.08	0.57	G	
103	990506A	A	CPL	$0.45^{+0.19}_{-0.20}$	-	414^{+37}_{-28}	4.45 ± 0.10	0.79	P	
103	990506A	B	CPL	$0.68^{+0.13}_{-0.14}$	-	256^{+9}_{-9}	6.23 ± 0.12	1.08	P	
104	990510	A	CPL	$1.25^{+0.24}_{-0.27}$	-	164^{+21}_{-17}	1.56 ± 0.09	0.45	W	
104	990510	B	POW	$1.54^{+0.83}_{-0.80}$	-	-	0.13 ± 0.06	0.75	W	
105	990518B	A	POW	$2.17^{+0.51}_{-0.48}$	-	-	0.22 ± 0.06	0.56	4B 7575	
105	990518B	B	CPL	$0.55^{+0.06}_{-0.07}$	-	432^{+16}_{-14}	9.66 ± 0.08	1.10	4B 7575	
110	990712A	A	POW	$1.30^{+0.17}_{-0.18}$	-	-	0.86 ± 0.08	0.66	4B 7647	
110	990712A	B	POW	$2.24^{+0.41}_{-0.40}$	-	-	0.33 ± 0.07	0.59	4B 7647	
112	990718	A	POW	$2.25^{+0.99}_{-0.85}$	-	-	0.21 ± 0.09	0.39	4B 7660	only unit 4 used
112	990718	B	CPL	$0.99^{+0.36}_{-0.41}$	-	251^{+39}_{-29}	1.74 ± 0.11	0.63	4B 7660	only unit 4 used
114	990726	A	POW	$1.79^{+0.22}_{-0.21}$	-	-	0.46 ± 0.06	0.83	G	
114	990726	B	POW	$1.97^{+0.21}_{-0.21}$	-	-	0.43 ± 0.06	0.63	G	
115	990907	A	POW	$1.93^{+0.19}_{-0.19}$	-	-	0.50 ± 0.06	0.63	W	
115	990907	B	POW	$1.85^{+0.24}_{-0.24}$	-	-	0.41 ± 0.06	0.58	W	
119	991116	A	CPL	$0.70^{+0.18}_{-0.19}$	-	283^{+28}_{-22}	2.28 ± 0.09	0.77	G	
119	991116	B	CPL	$0.82^{+0.26}_{-0.28}$	-	339^{+84}_{-49}	1.45 ± 0.08	0.63	G	
119	991116	C	POW	$2.25^{+0.71}_{-0.59}$	-	-	0.15 ± 0.05	0.50	G	
126	991226A	A	POW	$0.87^{+0.35}_{-0.41}$	-	-	1.35 ± 0.21	0.60	-	
126	991226A	B	POW	$1.92^{+1.32}_{-1.19}$	-	-	0.75 ± 0.35	0.68	-	

Table 3. continued.

# GRB	GRB	Interval	model	α	β	E_p (keV)	$\Phi(40-700)$ (10^{-5} erg cm^{-2})	χ^2/dof	CAT	comment
-	-	-	-	-	-	-	-	-	-	-
127	000104A[a]	A	-	-	-	-	-	-	-	
127	000104A	B	CPL	$1.09^{+0.42}_{-0.48}$	-	295^{+242}_{-66}	0.67 ± 0.06	0.73	4B 7933	
129	000109	A	CPL	$1.15^{+0.14}_{-0.15}$	-	366^{+75}_{-46}	3.09 ± 0.10	0.90	4B 7941	only unit 2 used, syst. deviat.
129	000109	B	CPL	$1.02^{+0.09}_{-0.09}$	-	> 596	6.00 ± 0.10	1.19	4B 7941	only unit 2 used, syst. deviat.
135	000218A	A	POW	$2.33^{+0.18}_{-0.17}$	-	-	1.03 ± 0.09	1.18	-	
135	000218A	B	POW	$2.65^{+0.35}_{-0.32}$	-	-	0.62 ± 0.10	0.67	-	
135	000218A	C	POW	$3.01^{+1.22}_{-0.84}$	-	-	0.27 ± 0.13	1.16	-	
136	000218B	A	POW	$1.06^{+0.12}_{-0.13}$	-	-	0.90 ± 0.05	0.74	-	
136	000218B	B	POW	$1.70^{+0.21}_{-0.21}$	-	-	0.52 ± 0.05	0.67	-	
137	000226	A	CPL (*)	$0.69^{+0.16}_{-0.16}$	-	342^{+29}_{-23}	3.37 ± 0.09	0.76	G	
137	000226	A	BAND	$-0.66^{+0.22}_{-0.20}$	[−2.3]	323^{+41}_{-34}	3.35 ± 0.09	0.78	G	
137	000226	B	CPL (*)	$0.87^{+0.09}_{-0.09}$	-	310^{+15}_{-13}	5.78 ± 0.08	0.91	G	
137	000226	B	BAND	$-0.80^{+0.13}_{-0.13}$	[−2.3]	284^{+22}_{-19}	5.77 ± 0.09	0.95	G	
138	000227	A	POW	$1.86^{+0.24}_{-0.24}$	-	-	0.60 ± 0.09	0.86	4B 8001	
138	000227	B	POW	$2.20^{+0.17}_{-0.16}$	-	-	0.89 ± 0.08	1.02	4B 8001	
139	000301C	A	POW	$2.05^{+0.29}_{-0.29}$	-	-	0.33 ± 0.06	1.02	G	
139	000301C	B	CPL	$0.60^{+0.42}_{-0.48}$	-	183^{+19}_{-16}	1.00 ± 0.07	0.51	G	
140	000312	A	POW (*)	$2.09^{+0.33}_{-0.32}$	-	-	0.27 ± 0.05	1.18	4B 8030	
140	000312	A	CPL	$-0.45^{+2.14}_{-3.05}$	-	144^{+54}_{-45}	0.21 ± 0.06	1.03	4B 8030	
140	000312	B	CPL	$0.84^{+0.59}_{-0.77}$	-	185^{+42}_{-30}	0.60 ± 0.07	0.74	4B 8030	
142	000327	A	POW	$1.76^{+0.31}_{-0.31}$	-	-	0.32 ± 0.06	0.64	G	
142	000327	B	CPL	$0.97^{+0.42}_{-0.48}$	-	223^{+63}_{-32}	0.88 ± 0.08	0.86	G	
143	000328	A	POW	$3.2^{-2.3}_{-2.3}$	-	-	0.08 ± 0.04	0.37	-	
143	000328	B	CPL	$1.19^{+0.63}_{-0.77}$	-	148^{+33}_{-57}	0.89 ± 0.09	0.82	-	
143	000328	C	POW	$4.42^{+0.71}_{-0.59}$	-	-	3.66 ± 1.25	0.67	-	only unit 2 used
146	000421	A	CPL	$-1.16^{+1.75}_{-2.77}$	-	170^{+24}_{-26}	0.74 ± 0.14	0.91	4B 8084	
146	000421	B	POW	$3.04^{+0.63}_{-0.55}$	-	-	0.59 ± 0.18	1.30	4B 8084	
147	000429	A	CPL	$0.80^{+0.21}_{-0.21}$	-	392^{+76}_{-42}	1.81 ± 0.06	0.72	I	
147	000429	B	POW	$1.82^{+0.30}_{-0.30}$	-	-	3.06 ± 0.05	0.56	I	
148	000523	A	CPL	$-0.27^{+0.66}_{-0.72}$	-	259^{+29}_{-23}	1.10 ± 0.10	0.82	-	
148	000523	B	POW	$2.03^{+1.44}_{-1.13}$	-	-	0.14 ± 0.08	0.82	-	
149	000528	A	CPL	$0.24^{+0.39}_{-0.45}$	-	175^{+16}_{-13}	0.97 ± 0.07	0.99	W	
149	000528	B	CPL	$0.81^{+0.78}_{-0.97}$	-	86^{+14}_{-29}	0.49 ± 0.05	0.54	W	
150	000615B[a]	A	-	-	-	-	-	-	-	
150	000615B	B	POW (*)	$1.84^{+0.19}_{-0.19}$	-	-	1.63 ± 0.18	0.67	I	
150	000615B	B	CPL	$0.89^{+0.78}_{-1.12}$	-	217^{+175}_{-53}	1.45 ± 0.24	0.56	I	
151	000621	A	CPL	[−1.0]	-	270^{+51}_{-42}	0.36 ± 0.05	0.76	G	
151	000621	B	CPL	$0.60^{+0.77}_{-0.95}$	-	239^{+37}_{-40}	0.91 ± 0.11	0.80	G	
155	000811[a]	A	-	-	-	-	-	-	-	
155	000811	B	CPL	$1.18^{+0.16}_{-0.17}$	-	248^{+20}_{-17}	3.01 ± 0.08	0.90	I	
160	001013	A	CPL	$1.28^{+0.17}_{-0.21}$	-	126^{+11}_{-11}	2.10 ± 0.08	1.01	G	
160	001013	B	POW	$2.50^{+0.17}_{-0.16}$	-	-	0.65 ± 0.06	0.87	G	
162	001110	A	POW (*)	$1.83^{+0.09}_{-0.09}$	-	-	1.24 ± 0.07	0.80	G	
162	001110	A	CPL	$1.40^{+0.32}_{-0.31}$	-	268^{+223}_{-59}	1.19 ± 0.08	0.75	G	
162	001110[a]	B	-	-	-	-	-	-	-	
163	001115	A	POW (*)	$1.71^{+0.34}_{-0.34}$	-	-	0.40 ± 0.08	0.80	G	
163	001115	A	CPL	< 1.3	-	281^{+175}_{-68}	0.34 ± 0.09	0.60	G	
163	001115	B	CPL	$0.17^{+1.00}_{-1.39}$	-	254^{+69}_{-43}	0.63 ± 0.10	0.61	G	
164	001206A	A	POW	$1.09^{+0.53}_{-0.60}$	-	-	0.18 ± 0.05	0.63	G	
164	001206A	B	CPL	$0.52^{+0.58}_{-0.74}$	-	177^{+37}_{-24}	0.53 ± 0.06	0.48	G	
165	001206C	A	POW	$1.08^{+0.51}_{-0.55}$	-	-	0.30 ± 0.08	0.45	G	
165	001206C	B	POW	$1.91^{+0.24}_{-0.24}$	-	-	0.47 ± 0.07	0.76	G	
168	001213	A	POW (*)	$2.35^{+0.72}_{-0.59}$	-	-	0.38 ± 0.13	1.77	-	
168	001213	A	CPL	< 1.71	-	169^{+68}_{-100}	0.30 ± 0.12	1.51	-	
168	001213[a]	B	-	-	-	-	-	-	-	
168	001213[a]	C	-	-	-	-	-	-	-	
168	001213	D	POW (*)	$2.14^{+0.27}_{-0.26}$	-	-	0.96 ± 0.13	1.38	-	
168	001213	D	CPL	$0.60^{+1.29}_{-1.94}$	-	164^{+59}_{-93}	0.81 ± 0.18	1.29	-	
168	001213	E	POW	$2.92^{+3.13}_{-1.24}$	-	-	0.32 ± 0.23	1.20	-	
169	001217	A	POW (*)	$2.16^{+0.26}_{-0.24}$	-	-	0.33 ± 0.05	0.85	G	
169	001217	A	CPL	$0.45^{+1.36}_{-2.13}$	-	117^{+38}_{-56}	0.27 ± 0.06	0.65	G	
169	001217[a]	B	-	-	-	-	-	-	-	
170	001219A	A	POW	$2.14^{+1.18}_{-0.98}$	-	-	0.29 ± 0.14	0.35	G	
170	001219A	B	POW	$2.29^{+0.30}_{-0.29}$	-	-	0.94 ± 0.15	0.57	G	
170	001219A	C	POW	$1.97^{+0.64}_{-0.62}$	-	-	0.38 ± 0.12	0.43	G	
174	010127	A	POW (*)	$1.80^{+0.14}_{-0.13}$	-	-	0.80 ± 0.06	0.84	-	

Table 3. continued.

# GRB	GRB	Interval	model	α	β	E_{p} (keV)	$\Phi(40-700)$ (10^{-5} erg cm^{-2})	χ^2/dof	CAT	comment
-	-	-	-	-	-	-	-	-	-	-
174	010127	A	CPL	$1.06^{+0.55}_{-0.66}$	-	294^{+217}_{-59}	0.73 ± 0.07	0.77	-	
174	010127	B	POW	$1.82^{+0.24}_{-0.24}$	-	-	0.47 ± 0.06	1.05	-	
176	010222A	A	POW	$1.96^{+0.15}_{-0.15}$	-	-	0.71 ± 0.05	0.76	W	
176	010222A	B	CPL	$1.15^{+0.06}_{-0.06}$	-	347^{+16}_{-14}	8.29 ± 0.09	0.96	W	
179	010324	A	POW (*)	$1.93^{+0.45}_{-0.41}$	-	-	0.18 ± 0.05	1.16	A	
179	010324	A	CPL	< 1.82	-	171^{+86}_{-46}	0.14 ± 0.05	0.76	A	
179	010324	B	CPL	$0.79^{+0.28}_{-0.31}$	-	241^{+34}_{-25}	1.12 ± 0.06	0.62	A	
179	010324	C	CPL	< 1.41	-	140^{+50}_{-37}	0.16 ± 0.05	0.65	A	
179	010324	C	POW (*)	$2.13^{+0.39}_{-0.37}$	-	-	0.20 ± 0.05	0.96	A	
179	010324	D	POW	$2.07^{+0.30}_{-0.28}$	-	-	0.28 ± 0.05	0.68	A	
179	010324	D	CPL	$0.93^{+1.07}_{-1.97}$	-	< 260	0.24 ± 0.06	0.58	A	
180	010326	A	POW (*)	$1.97^{+0.33}_{-0.33}$	-	-	0.40 ± 0.08	0.91	I	
180	010326	A	CPL	$0.60^{+1.37}_{-2.07}$	-	207^{+467}_{-133}	0.36 ± 0.09	0.84	I	
180	010326	B	POW (*)	$1.99^{+0.25}_{-0.26}$	-	-	0.52 ± 0.08	0.58	I	
180	010326	B	CPL	$0.93^{+1.04}_{-1.41}$	-	193^{+100}_{-58}	0.47 ± 0.09	0.52	I	
184	010427B	A	CPL	$0.84^{+0.11}_{-0.11}$	-	> 550	3.78 ± 0.06	0.92	G	
184	010427B	B	CPL	$1.12^{+0.19}_{-0.20}$	-	> 429	1.82 ± 0.06	0.67	G	
188	010619	A	CPL	$1.04^{+0.27}_{-0.31}$	-	185^{+22}_{-18}	1.32 ± 0.08	0.59	G	
188	010619[a]	B	-	-	-	-	-	-	-	
188	010619[b]	C	-	-	-	-	-	>3	-	
188	010619	D	POW	$1.85^{+0.29}_{-0.28}$	-	-	0.34 ± 0.06	0.86	G	
190	010711	A	POW	$2.49^{+0.23}_{-0.22}$	-	-	3.81 ± 0.49	0.89	-	
190	010711	B	POW	$2.64^{+0.91}_{-0.74}$	-	-	1.20 ± 0.47	0.69	-	
191	010715	A	POW	$2.48^{+0.81}_{-0.68}$	-	-	0.30 ± 0.11	0.75	-	
191	010715	B	POW	$2.25^{+0.36}_{-0.33}$	-	-	0.59 ± 0.10	0.39	-	
197	010826	A	CPL	$0.62^{+0.27}_{-0.29}$	-	277^{+35}_{-25}	1.32 ± 0.07	0.59	G	
197	010826	B	CPL	$0.75^{+0.24}_{-0.26}$	-	370^{+78}_{-47}	1.44 ± 0.07	0.69	G	
197	010826	C	POW	$1.92^{+0.24}_{-0.24}$	-	-	0.35 ± 0.05	0.75	G	

[a] Low signal, no useful spectrum.
[b] Unacceptable fit due to large χ^2.